

Incoherent transport on the $\nu = 2/3$ quantum Hall edge

Casey Nosiglia¹, Jinhong Park¹, Bernd Rosenow², Yuval Gefen^{1*}

¹*Dept. of Condensed Matter Physics, Weizmann Institute of Science, Rehovot 76100, Israel*

²*Institut für Theoretische Physik, Universität Leipzig, D-04103 Leipzig, Germany*

Abstract

The nature of edge state transport in quantum Hall systems has been studied intensely ever since Halperin [1] noted its importance for the quantization of the Hall conductance. Since then, there have been many developments in the study of edge states in the quantum Hall effect, including the prediction of multiple counter-propagating modes in the fractional quantum Hall regime, the prediction of edge mode renormalization due to disorder, and studies of how the sample confining potential affects the edge state structure (edge reconstruction), among others. In this paper, we study edge transport for the $\nu_{\text{bulk}} = 2/3$ edge in the disordered, fully incoherent transport regime. To do so, we use a hydrodynamic approximation for the calculation of voltage and temperature profiles along the edge of the sample. Within this formalism, we study two different bare mode structures with tunneling: the original edge structure predicted by Wen [2] and MacDonald [3], and the more complicated edge structure proposed by Meir [4], whose renormalization and transport characteristics were discussed by Wang, Meir and Gefen (WMG) [5]. We find that in the fully incoherent regime, the topological characteristics of transport (quantized electrical and heat conductance) are intact, with finite size corrections which are determined by the extent of equilibration. In particular, our calculation of conductance for the WMG model in a double QPC geometry reproduce conductance results of a recent experiment by Sabo et al. [21], which are inconsistent with the model of MacDonald. Our results can be explained in the charge/neutral mode picture, with incoherent analogues of the renormalization fixed points of Ref. [5]. Additionally, we find diffusive ($\sim 1/L$) conductivity corrections to the heat conductance in the fully incoherent regime for both models of the edge.

Keywords: Incoherent transport, fractional quantum Hall effect, edge states

1. Introduction

The edge states in a quantum Hall system play an essential role in defining the low energy dynamics of the system, specifically for low-frequency and d.c. transport [1]. In particular, the formation and remarkable quantization of Hall conductance plateaus in the integer quantum Hall effect (IQHE) and fractional quantum Hall effect (FQHE) provides evidence for transport through such gapless edge states, with localized states in the bulk. Furthermore, it was shown by Wen [6] that the gapless edge states consist of one-dimensional chiral bosonic modes, which are described in the framework of the Luttinger Liquid theory. These concepts have been successful in explaining transport properties in various quantum Hall geometries, including constrictions formed at quantum point contacts (QPCs) [7, 8, 9].

*yuval.gefen@weizman.ac.il

While one can easily characterize the edge states of the Laughlin series $1/(2m + 1)$ in terms of single branches of a chiral Luttinger Liquid, other fractional filling factors different from the Laughlin series are more complicated. A representative example of such a system is the hole-conjugate state $\nu_{\text{bulk}} = 2/3$. MacDonald [3], following an extension of the Haldane-Halperin hierarchy [10, 11], predicted the edge of the $\nu_{\text{bulk}} = 2/3$ state to consist of two counter-propagating modes, a “downstream” $\delta\nu = +1$ mode and an “upstream” $\delta\nu = -1/3$ mode, a picture that was corroborated by Wen [2] [see Fig. 1(a)]. However, this picture predicts a 2-terminal conductance of $G = (4/3)e^2/h$ universally, which is clearly in contradiction with the experimentally observed $G = (2/3)e^2/h$; additionally, the upstream $1/3$ mode was never detected [12]. The resolution of this problem was described in a pioneering paper of Kane, Fischer and Polchinski [13] (KFP), which considered random disorder-induced tunneling between the modes. Interplay between tunneling and the interaction drives the system into a disorder-dominated phase, described by a downstream charge mode $\delta\nu = +2/3$ and an upstream neutral mode, predicting a conductance of $G = (2/3)e^2/h$. These ideas have recently received experimental support with the discovery of neutral modes at several filling factors [14]. Additionally, neutral modes have attracted a lot of interest because they carry energy and a quantum number without carrying charge. Moreover, they may drastically suppress anyonic interference [15, 16], and are stable in the presence of a noisy environment, with the environment acting to renormalize the edge state tunneling exponents [17, 18].

Yet despite the experimental success of Ref. [14], a major observation contradicts the KFP analysis: the conductance through a quantum point contact exhibits a plateau at $G = (1/3)e^2/h$ as a function of the gate voltage of the QPC [19, 20, 21]. This, along with the evidence for neutral modes [14] and a crossover of the effective charge as a function of temperature [20] motivated Wang, Meir and Gefen (WMG) [5] to propose a different edge structure, based on earlier work of edge reconstruction in a shallow confining potential [4]. The proposed bare edge structure consists of four edge modes corresponding to filling factor discontinuities (from the bulk to the edge) of $\delta\nu = -1/3, +1, -1/3$, and $+1/3$ [see Fig. 1(b)]. Including interactions and disorder induced tunneling between channels, WMG apply renormalization group techniques [22] in a manner analogous to KFP, finding stable phases consisting of charge/neutral modes, which they argue account for the experimental observations cited above. In particular, in the case that the outermost edge is clearly decoupled from the inner three modes, WMG find an intermediate fixed point phase consisting of two downstream modes with $\delta\nu = +1/3, +1/3$ and two upstream neutral modes. At the intermediate fixed point, the emergence of the conductance plateau of $G = (1/3)e^2/h$ is clear since the outer-most mode is fully transmitted, while the inner three modes are fully reflected.

From the above experimental considerations, it is clear that the MacDonald edge structure does not provide the full picture of electrical transport, leaving the question of the correct edge structure for $\nu_{\text{bulk}} = 2/3$ unresolved. Here, we produce calculations for both the WMG and MacDonald models with disorder in the incoherent regime, where tunneling events are uncorrelated and phase interference effects are washed out. The approach of fully incoherent transport in FQH edges was first investigated by Kane and Fisher in the context of equilibration of the edge states with contacts [25]. In later works, it was shown that the incoherent regime is important for explaining conductance quantization in disordered quantum Hall edges near the KFP fixed point, whereas the comparable setting for the coherent regime exhibits mesoscopic conductance fluctuations which are dependent upon the disorder realization [23, 24]. Thus, the incoherent regime is essential for conductance quantization with charge and neutral modes. Previous works on the incoherent regime have only been done in the context of the MacDonald edge [23, 25, 26, 27]; our calculations in the incoherent regime provide evidence for the WMG model, qualitatively matching the results of a recent experiment [21] measuring electrical transport in a two QPC geometry.

Additionally, there has been increased experimental activity in the study of heat transport in the FQH regime

[30, 31, 32, 33], which is of interest for the study of neutral modes [34, 35, 36], and may prove a useful tool for characterizing the topological order in edge structures of various filling factors: for the $\nu_{\text{bulk}} = 5/2$ state, see Ref. [28, 29]. In particular, recent papers by Banerjee et al. [32, 37] report measurements of the thermal conductance for several different filling factors in the FQH regime. Motivated by this recent experimental progress, we study heat transport for the MacDonald and WMG models within the incoherent transport framework, applying it to the single QPC geometry.

There is also a recent theoretical paper [24] by one of the authors, which is a comprehensive study of the electrical and thermal conductances for the $\nu_{\text{bulk}} = 2/3$ state with counter-propagating $\delta\nu = +1$ and $\delta\nu = -1/3$ edges. This work provides a microscopic calculation for the thermal and electrical conductances, and examines their dependence on length and temperature near the KFP fixed point, and in the weakly interacting regime. The authors find that, beyond some length and temperature scales, incoherent transport becomes universal in both cases, and provide calculations for the electrical and thermal conductances in this regime. The present work extends the results of Ref. [24] in the incoherent regime in several respects. Beyond the two terminal setups examined in Ref. [24], we calculate the electrical and thermal conductances for the MacDonald model in several experimentally relevant geometries, including the line junction, low-density constriction, and a single QPC. We also calculate local temperature and voltage profiles $V_{1(\nu)}(x), T_{1(\nu)}(x)$ (where the index $1(\nu)$ indicates the filling factor discontinuity $\delta\nu = +1$ ($\delta\nu = -\nu$)), which provide some insight into how inter-channel equilibration occurs. In addition to the MacDonald model, we provide calculations for the WMG model which are directly relevant to experiment [21], as mentioned above. Furthermore, the downstream channel $\delta\nu = -1/3$ can be generalized to any Laughlin edge state, with $\delta\nu = -1/(2p + 1)$, for any positive integer p .

In addition to extending the calculations on incoherent transport in [24], the present work was partly inspired by previous papers on incoherent transport by several authors [23, 25, 26, 27], and our results overlap with some of these works. Overlap includes the form for the conductance of a single edge [23, 27], vanishing heat conductance with diffusive corrections [26], and a finite neutral mode decay length [25]. However, our work goes beyond the previously mentioned works in several respects. The new results of this work include:

- Electrical and thermal conductances for the MacDonald model in several geometries (line junction, low-density constriction, single QPC).
- Calculation of the local temperature and voltage profiles $V_{1(\nu)}(x), T_{1(\nu)}(x)$ in the line junction [see Fig. 2(b)], including the voltage induced temperature profiles. In particular, the voltage profiles have an exponential dependence on x , with exponential decay near $x = L$, rather than the usual Ohmic behavior in diffusive conductors [39]; this exponential decay near the drain reflects the presence of the neutral mode. Additionally, the voltage induced temperature profiles show rapid heating near the drain due to the presence of the neutral mode.
- Electrical conductances for the WMG model in the single and double QPC configurations with the outer-most channel fully transmitted. In particular, in the two QPC configuration we see the transition from $(1/3)e^2/h$ conductance to $(1/6)e^2/h$ conductance as a function of the separation of the QPCs, matching the experimental results of [21].
- Thermal conductance for the WMG model in the single QPC configuration with the outer-most channel fully transmitted. We also find vanishing thermal conductance with diffusive conductivity corrections ($\sim 1/L$), as previously noted in Ref. [26].

The organization of this article is as follows. In Section 2, we explain the basic assumptions of our incoherent model for the edge, and derive the steady state heat and electrical transport equations for the MacDonald edge,

with applications to various geometries. In Section 3, we apply the same formalism to the WMG edge in single and double QPC geometries. In Section 4, we summarize the results of the previous sections, and discuss the implications of our work and possible future directions.

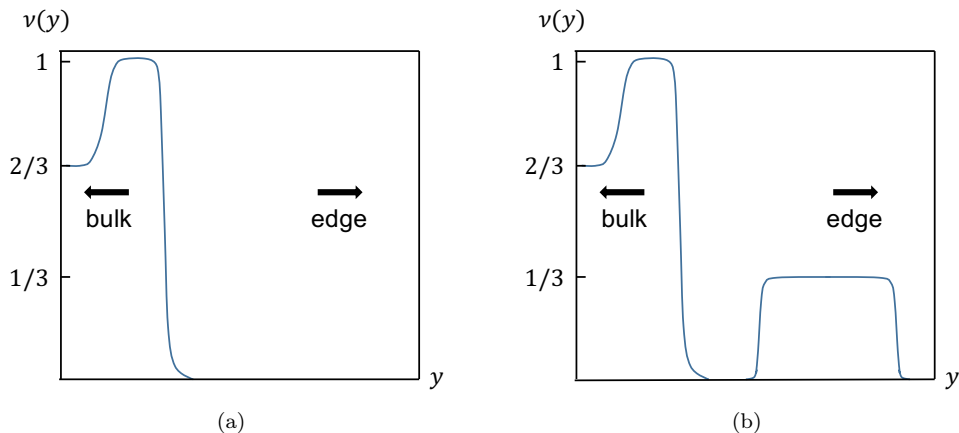


Figure 1: (a) Schematic plot of the filling factor $\nu(y)$ as a function of the coordinate y perpendicular to the edge for the KFP edge structure as proposed by MacDonald [3]. The boundary between regions of different filling factor are where the edge modes reside. (b) Filling factor $\nu(y)$ as a function of the coordinate y perpendicular to the edge for the WMG edge structure. Due to the shallow confining potential, a wide $\nu = 1/3$ incompressible strip is created near the edge of the sample [4, 5].

2. Description of the model (MacDonald edge with tunneling)

In this section, we study the steady state transport characteristics of counter-propagating $\delta\nu = +1$ and $\delta\nu = -\nu$ modes with impurity mediated tunneling between them. We treat the problem in the incoherent regime, where phase coherence and quantum interference effects between successive tunneling events are ignored. In addition, we assume that electrons equilibrate between tunneling events, resulting in local electrochemical potential $\mu_0 + eV_{1(\nu)}(x)$ and local temperature $T_{1(\nu)}(x)$ on the edge mode $1(\nu)$ [see Fig. 2(a)]. Here μ_0 is chemical potential in the absence of bias voltage. Effectively introducing local voltage and temperature probes between consecutive tunneling bridges on each edge mode, the local chemical potential and temperature are determined such that no net electric current and energy current flow between the system and the voltage contacts [40]. While we implicitly assume inelastic scattering within each mode to facilitate such equilibration, we take this as an assumption and will not specify any detailed mechanisms for equilibration in this paper. We note that while our general emphasis in this paper is on the $\nu_{\text{bulk}} = 2/3$ state, the calculations in this section can be applied to filling fractions of the form $\nu_{\text{bulk}} = 2p/(2p + 1)$, with positive integer p . We note that the results of this section may be relevant to recent experiments by Ronen et al. [41], who were able to engineer counter-propagating modes with tunable filling factors in both the integer and fractional quantum Hall regimes, using a double-quantum-well structure in a GaAs-based system.

symbol	short description	section
g	tunneling probability between counter-propagating $\delta\nu = +1, -\nu$ modes	2.1
a	separation between impurities	2.1
ℓ	scattering length	2.1
L	length of tunneling region	2.1
ν_0 (ν)	filling factor of the downstream (upstream) mode	2.1
T_0	ambient temperature	2.1
γ	deviation from the Wiedemann-Franz law at a single tunneling bridge	2.1
$\bar{\ell}$	modified scattering length	2.1
$\Delta V_{1(\nu)}, \Delta T_{1(\nu)}$	temperature and voltage biases applied to the corresponding sources	2.1
$\Delta I_{1(\nu)}, \Delta J_{1(\nu)}$	electrical and heat currents induced by biases at corresponding drains	2.1
$G_{S_{1(\nu)}D_{1(\nu)}}$	electrical conductances for voltage biasing at S_1, S_ν	2.1
$K_{S_{1(\nu)}, D_{1(\nu)}}$	thermal conductances for temperature biasing at S_1, S_ν	2.1
g_1 (g_2)	tunneling probability for current between inner-three (outer-two) modes	3.1
ℓ_1 (ℓ_2)	scattering lengths for inner-three (outer-two) modes	3.1
α	ratio of scattering lengths ℓ_1/ℓ_2	3.1
$\tilde{\gamma}$	deviation from the Wiedemann-Franz law at a single tunneling bridge for tunneling between $\delta\nu = +\nu, -\nu$ modes	3.1
$\bar{\ell}_1$ ($\bar{\ell}_2$)	scattering lengths for thermal transport for inner-three (outer-two) modes	3.1
$\bar{\alpha}$	ratio of modified scattering lengths $\bar{\ell}_1/\bar{\ell}_2$	3.1
L_V	width of QPC constriction	3.2
$G_{S_1, D_{2,3,4}}$	conductance from S_1 to drains	3.2
$K_{S_1, D_{2,3,4}}$	thermal conductance from S_1 to drains	3.2
K_{back}	thermal conductance of backscattered heat current	3.2
v_1	velocity of the upper ($\delta\nu = +1$) mode	app. A
v_ν	velocity of the lower ($\delta\nu = -\nu$) mode	app. A
Γ_0	tunneling strength at a single impurity	app. A
b	ultraviolet spatial cutoff	app. A

Table 1: List of symbols, their brief description, and the section where they are defined

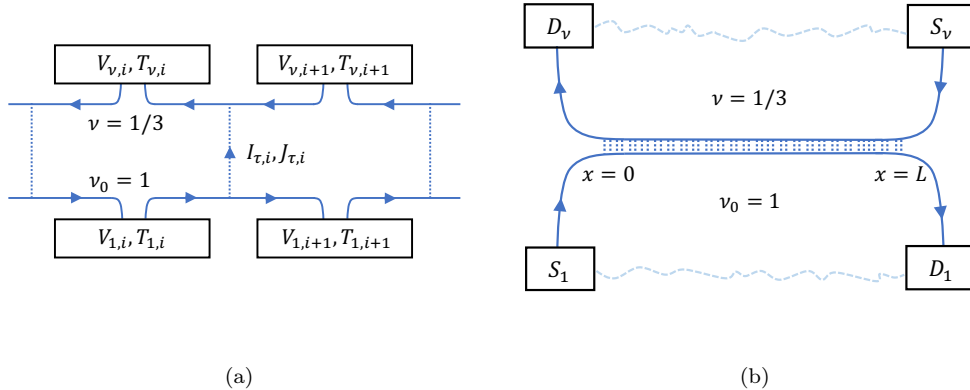


Figure 2: (a) Discrete tunneling bridge for calculation of the steady-state current/voltage distribution. The dashed line indicates the impurity-mediated tunneling, with associated currents $I_{\tau,i}, J_{\tau,i}$. The length of each segment i is a . The voltage and temperature of the probes are adjusted in such a way that no net electrical or thermal current flows between the probes and the edge. In this way the system equilibrates in between tunneling events, such that it can be characterized by a local chemical potential and temperature. (b) A line junction consisting of counter-propagating $\delta\nu = +1$ and $\delta\nu = -\nu$ edge modes, formed at the interface between $\nu_0 = 1$ and $\nu = 1/3$ FQH fluids. The heat/energy current can be injected at S_1 or S_ν and is measured at the drains. The dashed lines are schematic, indicating the continuation of the QH fluid not shown in the figure. The short dotted lines represent tunneling between the counter-propagating modes.

2.1. Derivation of transport equations and application to the line junction

We first take the simplest case of tunneling between counter-propagating 1 and ν modes in a line junction as our starting point [see Fig. 2(b)]. The model consists of tunneling bridges evenly spaced with separation a . For each segment, we impose the local constitutive relations for coupling voltage to current for each mode on a FQH edge:

$$\frac{e^2}{h}V_{1,i} = I_{1,i}, \quad -\nu\frac{e^2}{h}V_{\nu,i} = I_{\nu,i} \quad (1)$$

Additionally, we have conservation of current at each tunneling bridge, with our sign convention such that current flowing *downstream* on the 1-channel (we use the words “mode” and “channel” interchangeably) is positive, and current flowing *downstream* on the ν -channel is negative [see Fig. 2(a)]:

$$I_{1,i+1} = I_{1,i} - I_{\tau,i}, \quad I_{\nu,i} = I_{\nu,i+1} - I_{\tau,i}, \quad (2)$$

where $I_{\tau,i}$ is the tunneling current between segment i and $i+1$. The tunneling current is of the form:

$$I_{\tau,i} = g\frac{e^2}{h}(V_{1,i} - V_{\nu,i+1}), \quad (3)$$

where the coefficient g is the tunneling probability (see Appendix B). Applying Eqs. (1) and (3) to the conservation condition Eq. (2), we obtain the following iterative equations at a given tunneling bridge:

$$\frac{1}{(1-g/\nu)} \begin{pmatrix} [1-g(1+1/\nu)] & g \\ -g/\nu & 1 \end{pmatrix} \begin{pmatrix} V_{1,i} \\ V_{\nu,i} \end{pmatrix} = \begin{pmatrix} V_{1,i+1} \\ V_{\nu,i+1} \end{pmatrix} \quad (4)$$

Making use of the assumption that $g \ll 1$ by keeping terms only up to $O(g)$, taking the distance between impurities a as the smallest scale of variation (so that $ia \rightarrow x$) and taking the number of tunneling bridges $n \rightarrow \infty$, we obtain the following differential equations:

$$\frac{g}{a} \begin{pmatrix} -1 & 1 \\ -\nu^{-1} & \nu^{-1} \end{pmatrix} \begin{pmatrix} V_1(x) \\ V_\nu(x) \end{pmatrix} = \frac{d}{dx} \begin{pmatrix} V_1(x) \\ V_\nu(x) \end{pmatrix} \quad (5)$$

The eigenvectors and corresponding eigenvalues are $[(\nu^{-1} - 1)g/a, 0]$ and $\begin{pmatrix} 1 \\ \nu^{-1} \end{pmatrix}, \begin{pmatrix} 1 \\ 1 \end{pmatrix}$, respectively; thus the solution can be written in the form:

$$\vec{V}(x) = A \begin{pmatrix} 1 \\ \nu^{-1} \end{pmatrix} e^{\frac{(\nu^{-1}-1)gx}{a}} + B \begin{pmatrix} 1 \\ 1 \end{pmatrix} \quad (6)$$

Biasing the 1-channel by V_0 and grounding the ν -channel, we obtain the following solutions:

$$V_1(x) = \frac{V_0 \left(1 - \nu e^{\frac{(\nu^{-1}-1)(x-L)}{\ell}}\right)}{\left(1 - \nu e^{-\frac{(\nu^{-1}-1)L}{\ell}}\right)}, \quad V_\nu(x) = \frac{V_0 \left(1 - e^{\frac{(\nu^{-1}-1)(x-L)}{\ell}}\right)}{\left(1 - \nu e^{-\frac{(\nu^{-1}-1)L}{\ell}}\right)}, \quad (7)$$

where $\ell \equiv a/g$ is the scattering length, which also characterizes inter-channel equilibration of voltages. From this, we can easily calculate the conductance of the current transmitted from the source of the 1-channel to its drain [38]:

$$G_{S_1 D_1} = \frac{I_1(L)}{V_0} = \frac{e^2}{h} \frac{(1 - \nu)}{\left(1 - \nu e^{-\frac{(\nu^{-1}-1)L}{\ell}}\right)} \quad (8)$$

Additionally, we have the conductance of the current backscattered to the drain of the ν -channel:

$$G_{S_1 D_\nu} = \frac{|I_\nu(0)|}{V_0} = \nu \frac{e^2}{h} \frac{\left(1 - e^{-\frac{(\nu^{-1}-1)L}{\ell}}\right)}{\left(1 - \nu e^{-\frac{(\nu^{-1}-1)L}{\ell}}\right)}, \quad (9)$$

so that $G_{S_1 D_1} + G_{S_1 D_\nu} = e^2/h$, as required by current conservation. Here, we see that in the limit that $\ell \ll L$, we obtain near quantization of the transmitted and backscattered conductances, with exponentially small corrections: $G_{S_1 D_1} \approx (1 - \nu) (e^2/h) \left(1 + \nu e^{-\frac{(\nu^{-1}-1)L}{\ell}}\right)$, $G_{S_1 D_\nu} \approx \nu (e^2/h) \left(1 - (1 - \nu) e^{-\frac{(\nu^{-1}-1)L}{\ell}}\right)$.

We can perform a similar analysis for the temperature profiles induced by the applied voltage bias V_0 , through enforcing local conservation of energy. The energy tunneling current calculated from the Keldysh formalism (see Appendix B) is of the form:

$$J_{\tau,i} = g \frac{e^2}{2h} (V_{1,i}^2 - V_{\nu,i+1}^2) + \gamma g \frac{\pi^2 k^2}{6h} (T_{1,i}^2 - T_{\nu,i+1}^2), \quad (10)$$

where $\gamma \equiv 3/(2\nu+1) \xrightarrow{\nu \rightarrow 1/3} 9/5$ in the absence of interactions between the modes; γ is a constant which measures the deviation from the Wiedemann-Franz for the tunneling currents at a single impurity (see Appendix B), and

k is Boltzmann's constant. Additionally, we have the local constitutive relations for the energy current for each mode on the edge:

$$J_{1,i} = \frac{e^2}{h} \frac{V_{1,i}^2}{2} + \frac{\pi^2 k^2}{6h} T_{1,i}^2, \quad J_{\nu,i} = -\nu \frac{e^2}{h} \frac{V_{\nu,i}^2}{2} - \frac{\pi^2 k^2}{6h} T_{\nu,i}^2. \quad (11)$$

Applying conservation of energy current at each tunneling bridge, we obtain the following equations for the temperatures T_1, T_ν :

$$\frac{e^2}{h} \frac{V_{1,i+1}^2}{2} + \frac{\pi^2 k^2}{6h} T_{1,i+1}^2 = (1-g) \frac{e^2}{h} \frac{V_{1,i}^2}{2} + g \frac{e^2}{h} \frac{V_{\nu,i+1}^2}{2} + (1-\gamma g) \frac{\pi^2 k^2}{6h} T_{1,i}^2 + \gamma g \frac{\pi^2 k^2}{6h} T_{\nu,i+1}^2 \quad (12)$$

$$\nu \frac{e^2}{h} \frac{V_{\nu,i}^2}{2} + \frac{\pi^2 k^2}{6h} T_{\nu,i}^2 = (\nu-g) \frac{e^2}{h} \frac{V_{\nu,i+1}^2}{2} + g \frac{e^2}{h} \frac{V_{1,i}^2}{2} + (1-\gamma g) \frac{\pi^2 k^2}{6h} T_{\nu,i+1}^2 + \gamma g \frac{\pi^2 k^2}{6h} T_{1,i}^2 \quad (13)$$

Once again keeping terms only up to $O(g)$ and going to the continuum limit, we obtain the following differential equations:

$$\Rightarrow \partial_x \begin{pmatrix} T_1^2(x) \\ T_\nu^2(x) \end{pmatrix} = \frac{\gamma}{\ell} \begin{pmatrix} -1 & 1 \\ -1 & 1 \end{pmatrix} \begin{pmatrix} T_1^2(x) \\ T_\nu^2(x) \end{pmatrix} + \frac{1}{\ell} \frac{3e^2(V_\nu(x) - V_1(x))^2}{\pi^2 k^2} \begin{pmatrix} -1 \\ 1 \end{pmatrix} \quad (14)$$

These coupled differential equations are inhomogeneous linear differential equations (i.e. of the form $A\bar{x}(t) + \bar{f}(t) = \partial_t \bar{x}(t)$), and can be solved generally with a matrix exponential. The boundary conditions are specified by applying a voltage bias V_0 on either source S_1 or source S_ν in the presence of an ambient temperature T_0 . One finds that the difference $(V_\nu(x) - V_1(x))^2$ is the same in either case; the solution of Eq. (13) is thus the same for both cases, and is of the form:

$$\begin{aligned} T_1^2(x) &= T_0^2 + \frac{3\nu(eV_0/k)^2}{2\pi^2 \left(1 - \nu e^{-\frac{(\nu-1)L}{\ell}}\right)^2} \left\{ \frac{\gamma x}{\ell + \gamma L} \left[(1-\nu + \gamma\nu) + (1-\nu - \gamma\nu) e^{-\frac{2(\nu-1)L}{\ell}} \right] \right. \\ &\quad \left. + [1-\nu - \gamma\nu] \left[e^{\frac{2(\nu-1)(x-L)}{\ell}} - e^{-\frac{2(\nu-1)L}{\ell}} \right] \right\} \\ T_\nu^2(x) &= T_0^2 + \frac{3\nu(eV_0/k)^2}{2\pi^2 \left(1 - \nu e^{-\frac{(\nu-1)L}{\ell}}\right)^2} \left\{ \frac{\gamma(x-L)}{\ell + \gamma L} \left[(1-\nu + \gamma\nu) + (1-\nu - \gamma\nu) e^{-\frac{2(\nu-1)L}{\ell}} \right] \right. \\ &\quad \left. - [1-\nu + \gamma\nu] \left[e^{\frac{2(\nu-1)(x-L)}{\ell}} - 1 \right] \right\} \end{aligned} \quad (15)$$

With Eq. (14), we can also calculate heat transport along this edge in the presence of a temperature bias ΔT applied to the drain of the 1-channel, above an ambient temperature T_0 . Noting the form of the energy tunneling current (in the absence of a voltage bias V_0) at a tunneling bridge i , $J_{\tau,i} = \gamma g (\pi^2 k^2 / 6h) (T_{1,i}^2 - T_{\nu,i+1}^2)$, and the local constitutive relations for the heat current on a FQH edge as $J_{1,i} = (\pi^2 k^2 / 6h) T_{1,i}^2$, $J_{\nu,i} = -(\pi^2 k^2 / 6h) T_{\nu,i}^2$, we locally apply conservation of energy current at each tunneling bridge and obtain the following temperature

profiles:

$$\begin{aligned}
T_1^2(x) &= (T_0 + \Delta T)^2 - \Delta T(2T_0 + \Delta T) \frac{(x/\bar{\ell})}{(1 + L/\bar{\ell})}, \\
T_\nu^2(x) &= \frac{(T_0^2 + (L/\bar{\ell})(T_0 + \Delta T)^2)}{(1 + L/\bar{\ell})} - \Delta T(2T_0 + \Delta T) \frac{(x/\bar{\ell})}{(1 + L/\bar{\ell})},
\end{aligned} \tag{16}$$

with $\bar{\ell} \equiv \ell/\gamma$. Additionally, one can calculate the thermal conductances associated with the transmitted and backscattered heat currents:

$$K_{S_1 D_1} = \lim_{\Delta T \rightarrow 0} \frac{J_1(L, \Delta T + T_0) - J_1(L, T_0)}{\Delta T} = \frac{\pi^2 k^2 T_0}{3h} \frac{1}{(1 + L/\bar{\ell})}, \tag{17}$$

$$K_{S_1 D_\nu} = \lim_{\Delta T \rightarrow 0} \frac{J_\nu(0, \Delta T + T_0) - J_\nu(0, T_0)}{\Delta T} = \frac{\pi^2 k^2 T_0}{3h} \frac{L/\bar{\ell}}{(1 + L/\bar{\ell})}, \tag{18}$$

with $K_{S_1 D_1} + K_{S_1 D_\nu} = \pi^2 k^2 / 3h$, as required by conservation of energy. Finally, one can apply temperature and voltage biases to the 1 and ν -channel sources individually, described by a 4×4 linear response matrix:

$$\begin{pmatrix} \Delta I_1 \\ \Delta I_\nu \\ \Delta J_1 \\ \Delta J_\nu \end{pmatrix} = \begin{pmatrix} L_{11}^{11} & L_{11}^{12} & L_{12}^{11} & L_{12}^{12} \\ L_{11}^{21} & L_{11}^{22} & L_{12}^{21} & L_{12}^{22} \\ L_{21}^{11} & L_{21}^{12} & L_{22}^{11} & L_{22}^{12} \\ L_{21}^{21} & L_{21}^{22} & L_{22}^{21} & L_{22}^{22} \end{pmatrix} \begin{pmatrix} \Delta V_1 \\ \Delta V_\nu \\ \Delta T_1 \\ \Delta T_\nu \end{pmatrix}, \tag{19}$$

where $\Delta V_1, \Delta V_\nu, \Delta T_1, \Delta T_\nu$ are the individual biases on the drains and $\Delta I_1, \Delta I_\nu, \Delta J_1, \Delta J_\nu$ are the induced currents. The general form of the matrix turns out to be:

$$L = \begin{pmatrix} L_{11} & 0 \\ 0 & L_{22} \end{pmatrix}, \tag{20}$$

where the matrices L_{11} and L_{22} are of the form

$$L_{11} = \frac{e^2/h}{\left(1 - \nu e^{-\frac{(\nu^{-1}-1)L}{\bar{\ell}}}\right)} \begin{bmatrix} (1 - \nu) & \nu \left(1 - e^{-\frac{(\nu^{-1}-1)L}{\bar{\ell}}}\right) \\ \nu \left(1 - e^{-\frac{(\nu^{-1}-1)L}{\bar{\ell}}}\right) & \nu(1 - \nu) e^{-\frac{(\nu^{-1}-1)L}{\bar{\ell}}} \end{bmatrix}, \quad L_{22} = \frac{\pi^2 k^2}{3h} \frac{T_0}{(1 + L/\bar{\ell})} \begin{bmatrix} 1 & L/\bar{\ell} \\ L/\bar{\ell} & 1 \end{bmatrix}. \tag{21}$$

We see in the limit that $\bar{\ell}/L, \ell/L \rightarrow 0$, we obtain the following quantized values:

$$L_{11} = \frac{e^2}{h} \begin{bmatrix} (1 - \nu) & \nu \\ \nu & 0 \end{bmatrix}, \quad L_{22} = \frac{\pi^2 k^2}{3h} T_0 \begin{bmatrix} 0 & 1 \\ 1 & 0 \end{bmatrix}. \tag{22}$$

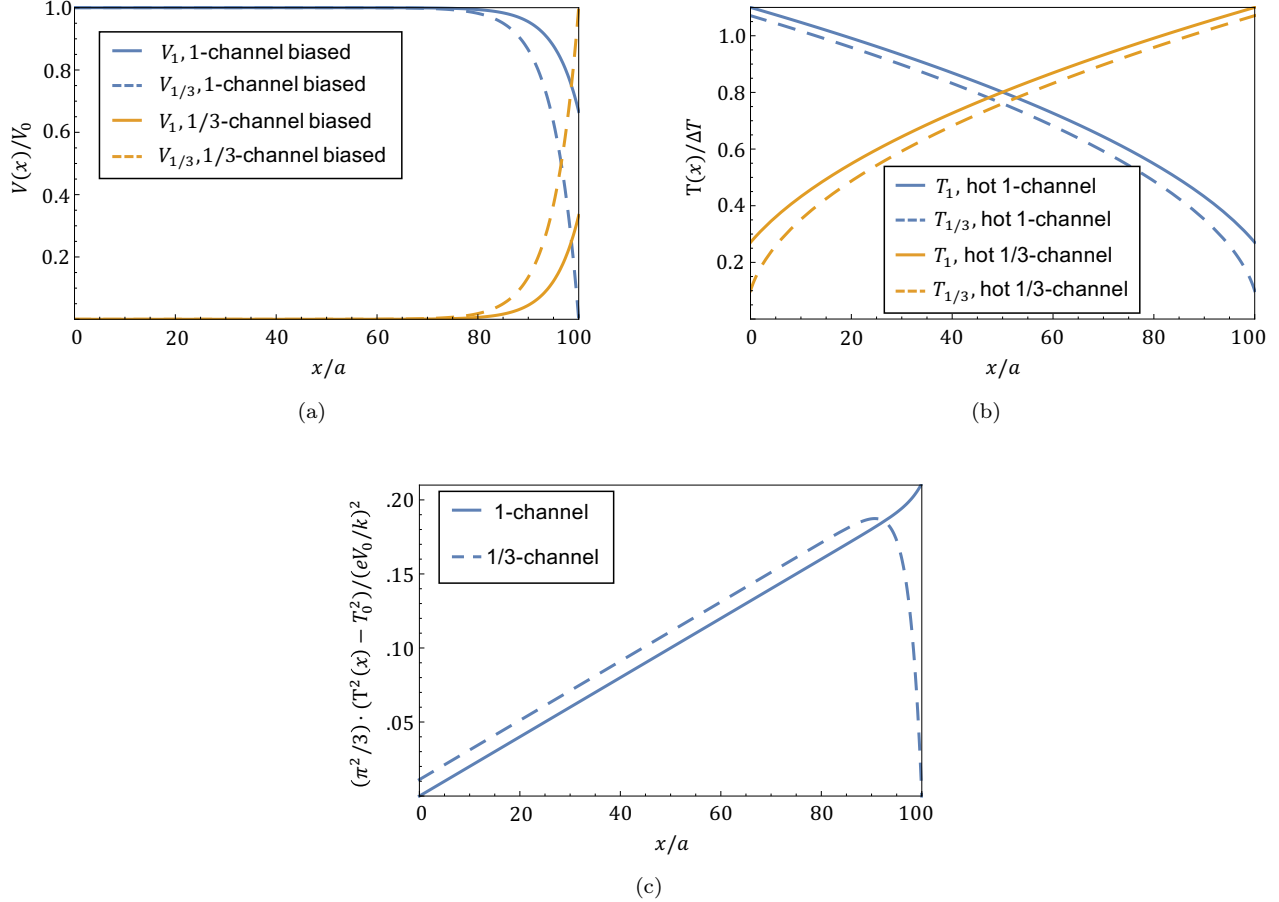


Figure 3: (a) Voltage profiles for the $1 - 1/3$ line junction, with $\ell = 10a, L = 100a$. We see explicitly that the equilibration of the two channels takes place within the length ℓ (b) Plot of the temperature profiles, with $\Delta T = 1, T_0 = .1, \bar{\ell} = 5.55a, L = 100a$ (c) Plot of the ratio of the net heat current to the total injected energy current $(\pi^2/3) \cdot (T^2(x) - T_0^2) / (eV_0/k)^2$ for $\ell = 10a, L = 100a$. This ratio is independent of the experimental parameters T_0, V_0 .

2.2. Discussion of line junction results

The results of the line junction calculations are shown in Figure 3. Fig. 3(a) shows the voltage profiles of Eq. (7) induced by an applied voltage V_0 . These profiles exhibit exponential decay near the drain, decaying with the scattering length ℓ , which characterizes inter-channel equilibration. Fig. 3(b) shows the temperature profiles of Eq. (16) induced by an applied temperature bias ΔT . These profiles exhibit inter-channel equilibration on a modified scale $\bar{\ell}$, but with power-law behavior which is characteristic of diffusive transport. Fig. 3(c) shows the ratio of the net heat current $J_{1,\nu} = (\pi^2 k^2 / 6h) (T_{1,\nu}^2(x) - T_0^2)$ induced by an applied voltage V_0 to the total injected energy current $(e^2 / 2h) V_0^2$ (the voltage-induced temperature profiles are given in Eq. (15)). The inter-channel equilibration is controlled by the scattering length ℓ , and we see that the ν channel is heated up near

the drain; these points are a reflection of the inter-channel equilibration of the voltages, which is the underlying mechanism for generating heat in this case.

It is interesting to contrast electrical transport in the case of counter-propagating $\delta\nu = +1$ and $\delta\nu = -\nu$ modes with that of counter-propagating $\delta\nu = +1$ and $\delta\nu = -1$ modes, which is the more familiar case of a quantum wire. In the $\delta\nu = +1$ and $\delta\nu = -1$ case, one finds that the voltage profiles are linear in x , and the conductance of the transmitted channel has a power-law decay as $G_{S_1 \rightarrow D_1} \sim \ell/L$, which is characteristic of diffusive Ohmic transport[39]:

$$V_{1,+}(x) = \frac{V_0}{(1 + L/\ell)} \left[1 + \left(\frac{L-x}{\ell} \right) \right], \quad V_{1,-}(x) = \frac{V_0}{(1 + L/\ell)} \left(\frac{L-x}{\ell} \right), \quad (23)$$

$$L_{11} = \frac{e^2/h}{(1 + L/\ell)} \begin{bmatrix} 1 & L/\ell \\ L/\ell & 1 \end{bmatrix}, \quad (24)$$

where $V_{1,+}(x)$ is the voltage profile associated with the downstream mode and $V_{1,-}(x)$ is the voltage profile associated with the upstream mode. However, if we look at Eqs. (8) and (21), we see an *exponential* dependence on x and exponentially small corrections to the quantized $(2/3)e^2/h$ value for the conductance, as mentioned before. Additionally, we can transform into the charge/neutral mode basis. Noting that the transformation into the charge and neutral mode basis is defined as $\phi_\rho = \phi_1 + \phi_\nu$, $\phi_\sigma = \phi_1 + \phi_\nu/\nu$, [5] the currents in the charge/neutral mode basis become (see Appendix E):

$$I_\rho \equiv I_1 + I_\nu = \frac{e^2}{h} V_0 \frac{(1-\nu)}{\left(1 - \nu e^{-\frac{(\nu^{-1}-1)L}{\ell}}\right)}, \quad I_\sigma \equiv I_1 + \frac{I_\nu}{\nu} = \frac{e^2}{h} V_0 \frac{(1-\nu)}{\left(1 - \nu e^{-\frac{(\nu^{-1}-1)L}{\ell}}\right)} e^{\frac{(\nu^{-1}-1)(x-L)}{\ell}}, \quad (25)$$

In this basis, we see that the charge mode is constant, reproducing the conductance of Eq. (8), and that the neutral mode decays exponentially from the drain to the source (see Fig. 3(a)); additionally, the direction of decay is predicted by the hierarchy scheme, as noted in Ref. [25]. The transformation into the charge/neutral basis can be given a more physical interpretation. The current corresponding to the charge field $\phi_\rho = \phi_1 + \phi_\nu$ is the total current $I_1 + I_\nu$, which is conserved along the line junction; note that this is not the total injected current $(e^2/h)V_0$ due to the backscattering to the drain of the ν -channel. The current corresponding to the neutral field $\phi_\sigma = \phi_1 + \phi_\nu/\nu$ is proportional to the tunneling current in the basis of the bare modes, i.e. $I_\sigma(x) = I_\tau(x)/g$; thus, in the incoherent regime, the decay of the current I_σ directly reflects the equilibration between the bare modes [25].

With regards to heat transport (see Fig. 3(b)), we note the same behavior (up to constants) in the 1 and 1 case as in the 1 and ν case, which is power-law dependence in the thermal conductance, with a slightly modified scattering length; thus in the limit of $\bar{\ell}/L \rightarrow \infty$, we have a vanishing thermal conductance but diffusive ($\sim 1/L$) thermal *conductivity* corrections.

We also note that the off-diagonal terms (thermoelectric contributions) are identically 0. At the individual tunneling bridge level, there are no L_{12} (electrical current induced by temperature difference) components due to the linearization of the electron energy spectrum (See Appendix B). We can see this because a temperature bias induces electron-hole excitations, and if the spectra of the channels are linear, there is no current generated, i.e. $\Delta I_1 = \Delta I_\nu = 0 \rightarrow \Delta I_\tau = 0$; this is more generally a reflection of the fact that the spectra have particle-hole symmetry. That the L_{21} elements (heat current induced by voltage difference) are identically zero can be seen as a consequence of Onsager symmetry.

We also note the voltage-induced temperature profiles (see Fig. 3(c)) are different from the typical profile in a diffusive conductor, where temperature scales as $T^2(x) \propto x(L-x)$ [39]. The spatial dependence of our

calculated temperature profiles scales as $T^2(x) \sim x$, with exponential corrections within a length $\sim \ell$ from the drain. Noting that the inhomogeneous term in Eq. (14) is proportional to I_σ^2 , we see that the exponential corrections reflect the decay of the neutral mode from the drain.

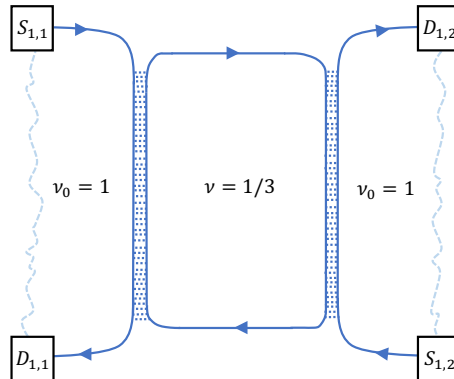


Figure 4: Geometry of a low-density constriction.

2.3. Low-density constriction and single-QPC geometries

To make a connection with a more common experimental setup and with the work of Ref. [23], we studied the same problem in a constriction geometry [see Fig. 4]. In this geometry, the filling factor ν_C in the constriction is less than that of the bulk ν_B , leading to tunneling at the interface of the two QH droplets in a manner similar to the problem of the counter-propagating $\nu_0 = 1$ and ν modes; this is a possible model for a QPC. Our setup matches with Fig. 1(b) of Ref. [23], with the exception that we do not consider inter-edge scattering across the constricted QH droplet. All of the machinery from the previous section is applicable here; the problem is effectively that of two coupled line junctions, where the ν modes are connected through the boundary conditions on their ends. Applying the appropriate boundary conditions, we calculate the response matrix L :

$$L_{12} = L_{21} = 0, \quad L_{11} = \frac{e^2/h}{\left(1 + e^{\frac{(\nu^{-1}-1)L}{\ell}} - 2\nu\right)} \begin{bmatrix} (1-\nu) \left(1 + e^{\frac{(\nu^{-1}-1)L}{\ell}}\right) & \nu \left(-1 + e^{\frac{(\nu^{-1}-1)L}{\ell}}\right) \\ \nu \left(-1 + e^{\frac{(\nu^{-1}-1)L}{\ell}}\right) & (1-\nu) \left(1 + e^{\frac{(\nu^{-1}-1)L}{\ell}}\right) \end{bmatrix},$$

$$L_{22} = \frac{\pi^2 k^2}{3h \left(1 + \frac{L/\bar{\ell}}{2}\right)} \begin{bmatrix} 1 & L/\bar{\ell} \\ L/\bar{\ell} & 1 \end{bmatrix} \quad (26)$$

We see that the results are very similar to those of the line junction in the 1-biased case; they conform to the same quantized values for heat and electrical conductance in the $\ell/L, \bar{\ell}/L \rightarrow 0$ limit, and the finite-size corrections have the same scaling with $\ell/L, \bar{\ell}/L$ as in the 1-biased case.

3. The WMG edge

In this section, we extend our results to the WMG edge, analyzing the single and double QPC geometries with only the outermost channel transmitted. Since the KFP picture cannot account for the $G = (1/3)e^2/h$

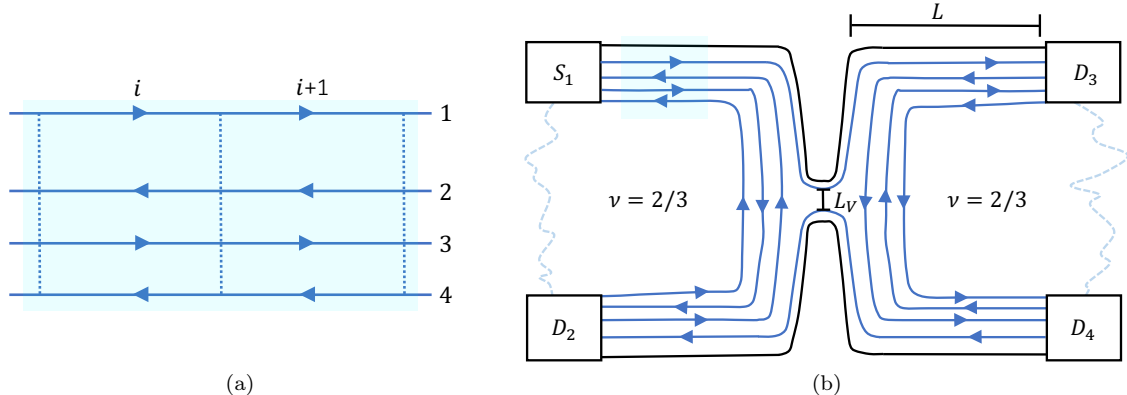


Figure 5: (a) Discrete tunneling bridge for the WMG edge structure. The inner three channels are characterized by the tunneling probability g_1 , while the outer-channel processes are characterized by the tunneling parameter g_2 (b) WMG edge structure in the QPC geometry (tunneling not shown)

conductance plateau [19, 20, 21] in a QPC, analysis of the WMG edge here becomes more relevant and gives rise to several different behaviors. Additionally, the recent transport experiment by Sabo et al. [21] in a two QPC geometry shows a conductance crossover from $(1/3)e^2/h$ to $(1/6)e^2/h$ as a function of the separation between the QPCs, which cannot be explained in the more conventional MacDonald picture and provides the impetus for studying the WMG model in this geometry. We also examine heat transport in the single QPC and compare the results to the MacDonald model.

3.1. Derivation of the transport equations

Electrical transport

We now generalize our calculations to the WMG picture of the edge. In this scheme, we take the bare modes of the WMG picture as a starting point (labelling the outermost mode 1, and the inner modes 2, 3, 4 from the edge to the bulk [see Fig. 5(a)]), and add single-electron tunneling processes between inner counter-propagating modes, in addition to a two-electron process which involves all three inner modes. The operators for these processes are of the form $\hat{O}_i = e^{i \sum_m n_{i,m} \cdot \phi_m}$, where $\phi_{m=2,3,4}$ are boson fields describing the inner-three modes, and the vectors \mathbf{n}_i are of the following form [5]:

$$\mathbf{n}_1 = \begin{pmatrix} 3 \\ 1 \\ 0 \end{pmatrix}, \mathbf{n}_2 = \begin{pmatrix} 0 \\ 1 \\ 3 \end{pmatrix}, \mathbf{n}_3 = \begin{pmatrix} 3 \\ 2 \\ 3 \end{pmatrix}. \quad (27)$$

While in principle these different processes will all have different tunneling probabilities $g_{n_1}, g_{n_2}, g_{n_3}$ associated with them, for simplicity we take the associated tunneling coefficients to all be the same magnitude, $g_1 \ll 1$, where g_1 is the probability for tunneling for the inner-three mode processes. In addition, we couple mode 1 to mode 2 through $1/3$ -charged quasiparticle tunneling, which has the form $I_{\tau 1,2,i} = g_2 (e^2/h) (V_{1,i} - V_{2,i+1})$, $g_2 \ll 1$, where g_2 is the probability for $1/3$ -charged quasiparticle tunneling. From here, we can now derive the

transport equations. We first divide the current into normal current and tunneling current as before:

$$\begin{aligned}
I_{1,i+1} &= I_{1,i} - I_{\tau 1,i} \\
I_{2,i+1} &= I_{2,i} - I_{\tau 2,i} \\
I_{3,i+1} &= I_{3,i} - I_{\tau 3,i} \\
I_{4,i+1} &= I_{4,i} - I_{\tau 4,i}
\end{aligned} \tag{28}$$

From current conservation, we must have that

$$I_{\tau 1,i} + I_{\tau 2,i} + I_{\tau 3,i} + I_{\tau 4,i} = 0 \tag{29}$$

and in particular, for any individual tunneling process, we must also have current conservation, e.g.

$$I_{n_3 2,i} + I_{n_3 3,i} + I_{n_3 4,i} = 0, \tag{30}$$

where $I_{n_3 2,i}$ is the tunneling current from channel 2 associated with the \mathbf{n}_3 process. The tunneling processes $\mathbf{n}_1, \mathbf{n}_2$ are simply the same tunneling processes we accounted for in the discussion of the KFP edge, and therefore have the same form for the tunneling current. However, \mathbf{n}_3 is a two-electron process and is more complicated. The tunneling current $I_{n_3 3,i}$ is of the following form:

$$I_{n_3 3,i} = \left(2g_1 \frac{e^2}{h} \right) \times [(V_{3,i} - V_{2,i+1}) + (V_{3,i} - V_{4,i+1})], \tag{31}$$

where the factor of 2 comes from the fact that it is a two-electron process [25]. With the use of Eq. (28), we can now write down the current conservation equations:

$$\begin{aligned}
I_{1,i+1} &= I_{1,i} - g_2 \frac{e^2}{3h} (V_{1,i} - V_{2,i+1}) \\
I_{2,i+1} &= I_{2,i} + g_2 \frac{e^2}{3h} (V_{1,i} - V_{2,i+1}) - g_1 \frac{e^2}{h} (V_{2,i+1} - V_{3,i}) - g_1 \frac{e^2}{h} (V_{2,i+1} - 2V_{3,i} + V_{4,i+1}) \\
I_{3,i+1} &= I_{3,i} + g_1 \frac{e^2}{h} (V_{2,i+1} - V_{3,i}) + 2g_1 \frac{e^2}{h} (V_{2,i+1} - 2V_{3,i} + V_{4,i+1}) + g_1 \frac{e^2}{h} (V_{4,i+1} - V_{3,i}) \\
I_{4,i+1} &= I_{4,i} - g_1 \frac{e^2}{h} (V_{4,i+1} - V_{3,i}) - g_1 \frac{e^2}{h} (V_{2,i+1} - 2V_{3,i} + V_{4,i+1})
\end{aligned} \tag{32}$$

Converting voltages to currents and taking the continuum limit, we obtain the following differential equations:

$$\frac{1}{\ell_1} \begin{pmatrix} -\alpha & -\alpha & 0 & 0 \\ \alpha & (\alpha + 6) & 3 & 3 \\ 0 & -9 & -6 & -9 \\ 0 & 3 & 3 & 6 \end{pmatrix} \begin{pmatrix} I_1(x) \\ I_2(x) \\ I_3(x) \\ I_4(x) \end{pmatrix} = \partial_x \begin{pmatrix} I_1(x) \\ I_2(x) \\ I_3(x) \\ I_4(x) \end{pmatrix}, \tag{33}$$

with $\ell_1 \equiv a/g_1, \ell_2 \equiv a/g_2, \alpha \equiv \ell_1/\ell_2$. From (33), one can directly see that current conservation is obeyed, i.e.

$\partial_x [I_1(x) + I_2(x) + I_3(x) + I_4(x)] = 0$. The solution to the differential equations (33) is of the form

$$\begin{aligned} \vec{I}(x) = & a_1 \begin{pmatrix} 0 \\ 0 \\ -1 \\ 1 \end{pmatrix} e^{\frac{3x}{\ell_1}} + a_2 \begin{pmatrix} -1 \\ 1 \\ -3 \\ 1 \end{pmatrix} + a_3 \begin{pmatrix} \frac{1}{6} \left(3 + \sqrt{3(3+8\alpha)} \right) \\ \frac{1}{6} \left(9 - \sqrt{3(3+8\alpha)} \right) \\ -3 \\ 1 \end{pmatrix} e^{\frac{1}{2} \left(3 - \sqrt{3(3+8\alpha)} \right) \frac{x}{\ell_1}} \\ & + a_4 \begin{pmatrix} \frac{1}{6} \left(3 - \sqrt{3(3+8\alpha)} \right) \\ \frac{1}{6} \left(9 + \sqrt{3(3+8\alpha)} \right) \\ -3 \\ 1 \end{pmatrix} e^{\frac{1}{2} \left(3 + \sqrt{3(3+8\alpha)} \right) \frac{x}{\ell_1}}, \end{aligned} \quad (34)$$

where a_1, a_2, a_3, a_4 are constants to be determined by the boundary conditions. In addition, for the analysis of the QPC with the outermost channel transmitted, we need the solution for the inner-three channel mixing without any coupling to the outermost mode:

$$\begin{aligned} \frac{1}{\ell_1} \begin{pmatrix} 6 & 3 & 3 \\ -9 & -6 & -9 \\ 3 & 3 & 6 \end{pmatrix} \begin{pmatrix} I_2 \\ I_3 \\ I_4 \end{pmatrix} &= \partial_x \begin{pmatrix} I_2 \\ I_3 \\ I_4 \end{pmatrix} \\ \Rightarrow \begin{pmatrix} I_2(x) \\ I_3(x) \\ I_4(x) \end{pmatrix} &= b_1 \begin{pmatrix} -1 \\ 0 \\ 1 \end{pmatrix} e^{\frac{3x}{\ell_1}} + b_2 \begin{pmatrix} -1 \\ 1 \\ 0 \end{pmatrix} e^{\frac{3x}{\ell_1}} + b_3 \begin{pmatrix} 1 \\ -3 \\ 1 \end{pmatrix}, \end{aligned} \quad (35)$$

where b_1, b_2, b_3 are constants to be determined by boundary conditions.

Charge/neutral mode basis

The differential equation Eq. (33) can be transformed into the corresponding charge/neutral mode basis for $\alpha = 0$ (i.e. the charge/neutral mode basis for the inner-three modes, as in Ref. [5]); this corresponds to obtaining the diagonal matrix $D = UAU^{-1}$:

$$A\vec{I} = \partial_x \vec{I} \rightarrow D\vec{\tilde{I}} = \partial_x \vec{\tilde{I}}, \quad (36)$$

with $\vec{\tilde{I}} = U^{-1}\vec{I}$. At the level of the ϕ fields, this corresponds to the transformation $\tilde{\phi}_i = (U^{-1})_{ij} \phi_j$, where $\tilde{\phi}_i$ are the new fields in the charge/neutral mode basis. For $\alpha = 0$, D and $(U_{ij})^{-1}$ are given as:

$$D = \text{diag} \left[\frac{3}{\ell_1}, \frac{3}{\ell_1}, 0, 0 \right], (U^{-1})_{ij} = \begin{pmatrix} 0 & 1 & 1 & 2 \\ 0 & 3 & 2 & 3 \\ 0 & 1 & 1 & 1 \\ 1 & 0 & 0 & 0 \end{pmatrix} \quad (37)$$

The first two rows correspond to the transformations for the neutral modes (with a finite decay length $\ell_1/3$), while the latter two correspond to the transformations for the charge modes (with eigenvalue 0); the neutrality of the neutral modes can be established by the fact that the creation operators carry zero net charge

(See Appendix A). The diagonal basis thus corresponds to the incoherent analogue of the intermediate fixed point.

We can also find the incoherent analogue of the KFP fixed point by looking at the $\alpha \rightarrow \infty$ limit. Diagonalizing the matrix of Eq. (30), we get the following solution:

$$\vec{I}(x) = a_1 \begin{pmatrix} 1 \\ 0 \\ 0 \\ 0 \end{pmatrix} e^{\frac{3x}{\ell_1}} + a_2 \begin{pmatrix} 0 \\ 1 \\ 0 \\ 0 \end{pmatrix} + a_3 \begin{pmatrix} 0 \\ 0 \\ 1 \\ 0 \end{pmatrix} e^{\frac{(3-\sqrt{3(3+8\alpha)})x}{2\ell_1}} + a_4 \begin{pmatrix} 0 \\ 0 \\ 0 \\ 1 \end{pmatrix} e^{\frac{(3+\sqrt{3(3+8\alpha)})x}{2\ell_1}}. \quad (38)$$

In the case where $\alpha \rightarrow \infty$ (by fixing ℓ_1 and taking $\ell_2 \rightarrow 0$), modes 3 and 4 in the new basis become completely localized near the boundaries, while mode 1 is a neutral mode with decay length $\ell_1/3$ and mode 2 is a charge mode.

Heat transport

In the case of heat transport, we find the following form of the tunneling current between counter-propagating $\delta\nu = +1$ and $\delta\nu = -\nu$ modes, and between counter-propagating $\delta\nu = +\nu$ and $\delta\nu = -\nu$ modes:

$$J_{\tau\nu_1-\nu_2,i} = \tilde{\gamma}g_2 \frac{\pi^2 k^2}{6h} (T_{\nu_1,i}^2 - T_{\nu_2,i+1}^2), \quad J_{\tau 1-\nu,i} = \gamma g_1 \frac{\pi^2 k^2}{6h} (T_{1,i}^2 - T_{\nu,i+1}^2), \quad (39)$$

with $\tilde{\gamma} \equiv 3\nu/(2\nu + 1) \xrightarrow{\nu \rightarrow 1/3} 3/5$ in the absence of interaction between the modes and γ as before; $\tilde{\gamma}$ is a constant which measures the deviation from the Wiedemann-Franz law for the tunneling current at a single impurity in the case of counter-propagating $\delta\nu = +\nu$ and $\delta\nu = -\nu$ modes (see Appendix B). For the \mathbf{n}_3 process, we assume the following form for the tunneling current:

$$J_{\tau 3,i}^{\mathbf{n}_3} = A(\bar{T}_i)(T_{3,i}^2 - T_{2,i+1}^2) + B(\bar{T}_i)(T_{3,i}^2 - T_{4,i+1}^2), \quad (40)$$

where the coefficients $A(\bar{T}_i), B(\bar{T}_i)$ can in principle have temperature dependence, with \bar{T}_i as the average temperature of the incoming modes at a tunneling bridge. We come to this form through the following considerations. We expect the heat tunneling current to depend on the difference of the squares of the temperatures of the individual modes, since heat current should depend on the square of the temperature, and should not have a contribution if adjacent channels have the same temperature. Also, by the symmetry of the problem, we set $A = B$, and as a simplifying assumption, $A = B = \gamma g_1$. The coefficients can in principle be different, and without doing a microscopic calculation we cannot know their form precisely, but since we are interested broadly in seeing the behavior of equilibration, we suspect that minute changes in the coefficients will not make much difference in the overall behavior of the system.

Putting this all together, we obtain the following equations for heat transport:

$$\frac{\gamma}{\ell_1} \begin{bmatrix} -\bar{\alpha} & \bar{\alpha} & 0 & 0 \\ -\bar{\alpha} & (\frac{3}{2} + \bar{\alpha}) & -2 & \frac{1}{2} \\ 0 & 2 & -4 & 2 \\ 0 & \frac{1}{2} & -2 & \frac{3}{2} \end{bmatrix} \begin{bmatrix} T_1^2(x) \\ T_2^2(x) \\ T_3^2(x) \\ T_4^2(x) \end{bmatrix} = \partial_x \begin{bmatrix} T_1^2(x) \\ T_2^2(x) \\ T_3^2(x) \\ T_4^2(x) \end{bmatrix}, \quad \frac{\gamma}{\ell_1} \begin{bmatrix} \frac{3}{2} & -2 & \frac{1}{2} \\ 2 & -4 & 2 \\ \frac{1}{2} & -2 & \frac{3}{2} \end{bmatrix} \begin{bmatrix} T_2^2(x) \\ T_3^2(x) \\ T_4^2(x) \end{bmatrix} = \partial_x \begin{bmatrix} T_2^2(x) \\ T_3^2(x) \\ T_4^2(x) \end{bmatrix}, \quad (41)$$

for the four-channel and three-channel mixing, respectively, where $\bar{\alpha} \equiv (\tilde{\gamma}/\gamma)\alpha = (\tilde{\gamma}/\gamma)\ell_1/\ell_2$. Taking into account the chirality of the channels, from Eqs. (38) one can easily see that energy is conserved. The resulting

solutions are

$$\begin{aligned}
\vec{T}^{\rightarrow}(x) &= c_1 \begin{pmatrix} 1 \\ 1 \\ 1 \\ 1 \end{pmatrix} + c_2 \left[\frac{x}{\ell_1} \begin{pmatrix} 1 \\ 1 \\ 1 \\ 1 \end{pmatrix} - \frac{1}{\bar{\alpha}\eta} \begin{pmatrix} (1+\bar{\alpha}) \\ \bar{\alpha} \\ 3\bar{\alpha}/4 \\ 0 \end{pmatrix} \right] + \frac{c_3}{(9+\eta)} \begin{pmatrix} -6\bar{\alpha} \\ 3-6\bar{\alpha}+3\eta \\ 4(3+\eta) \\ (9+\eta) \end{pmatrix} e^{\frac{-(1+\eta)\gamma x}{2\ell_1}} \\
&+ \frac{c_4}{(-9+\eta)} \begin{pmatrix} 6\bar{\alpha} \\ -3+6\bar{\alpha}+3\eta \\ 4(-3+\eta) \\ (-9+\eta) \end{pmatrix} e^{\frac{(-1+\eta)\gamma x}{2\ell_1}}, \\
\vec{T}^{\rightarrow}(x) &= d_1 \begin{pmatrix} 1 \\ 2 \\ 1 \end{pmatrix} e^{\frac{-2\gamma x}{\ell_1}} + d_2 \begin{pmatrix} -1 \\ 0 \\ 1 \end{pmatrix} e^{\frac{\gamma x}{\ell_1}} + d_3 \begin{pmatrix} 1 \\ 1 \\ 1 \end{pmatrix}, \tag{42}
\end{aligned}$$

with $\eta \equiv \sqrt{9+6\bar{\alpha}}$ and $c_1, c_2, c_3, c_4, d_1, d_2, d_3$ to be determined by the boundary conditions.

3.2. Transport in a single QPC

Electrical transport

The problem is now to match the boundary conditions to conform with the geometry of the QPC with the outermost channel transmitted [see Fig. 5(b)]. This requires matching 22 boundary conditions, which in principle is straightforward but leaves us with lengthy analytical expressions (see Appendix D). We numerically solve this linear system of 22 equations in 22 variables for different values of the parameters L, L_V, ℓ_1, ℓ_2 and examine the conductances $G_{S_1D_2}, G_{S_1D_3}, G_{S_1D_4}$ as functions of these parameters, where L_V is vertical separation of transmitted channels in the QPC, L is the length of an arm of the QPC, and ℓ_1, ℓ_2 are the scattering lengths associated with the inner three channels and the outer channel tunneling, respectively. We note that the following discussion is always in the regime where $\ell_1 \ll L$. Within this regime, we always have the condition that $G_{S_1D_2} + G_{S_1D_3} = (2/3)e^2/h$ (up to exponentially small corrections in L/ℓ_1); we see numerically that this condition is met.

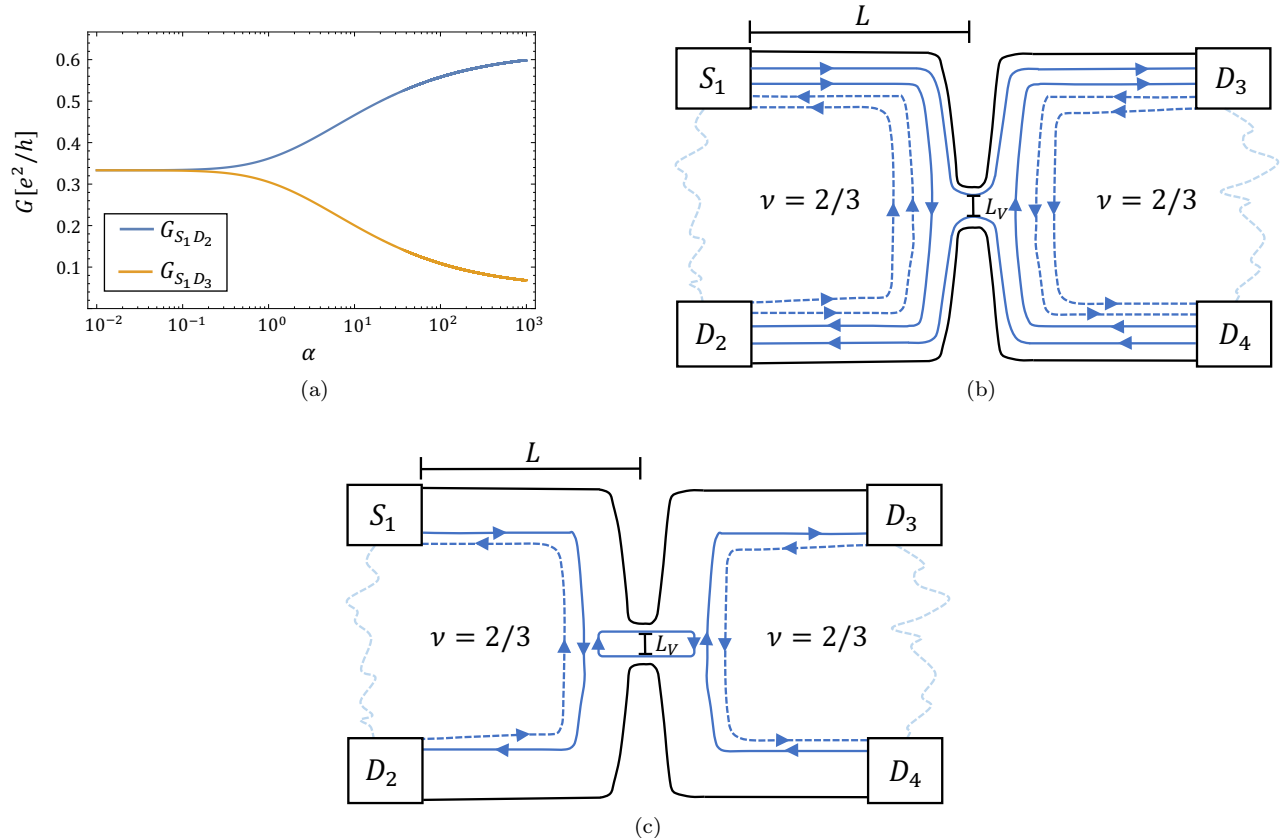


Figure 6: (a) Linear-log plot of the conductances $G_{S_1 D_2}, G_{S_1 D_3}$ in the single QPC as a function of $\alpha = \ell_1/\ell_2$ for $\ell_1 = 100a, L = 1000a, L_V = 5a$, and $\alpha = .01 - 1000$. (b) Renormalized edge modes of the single QPC at the intermediate fixed point. This renormalized edge structure picture produces conductance results qualitatively similar to our model in the regime that $\ell_2 > L$ (the decay of the neutral modes is not shown). (c) Renormalized edge modes of the single QPC in the KFP (low-temperature) fixed point, with a $\nu = 1/3$ density QH droplet in the constriction. This renormalized edge structure picture produces conductance results qualitatively similar to our model in the limit that $\alpha \rightarrow \infty$ (the decay of the neutral mode is not shown).

Results

The results of the calculation can be characterized by several different classes of behavior depending on the ratios of the lengths L, L_V, ℓ_1 , and ℓ_2 . We note that out of the six possible ratios of the length scales $(\alpha, \ell_1/L, \ell_1/L_V, \ell_2/L, \ell_2/L_V, L/L_V)$, the ratios which show up directly in the equations are $\alpha, \ell_1/L, \ell_1/L_V, \ell_2/L$; we choose these as our parameters to span parameter space. Then, the parameters that we play with are $\alpha, \ell_1/L_V$, and ℓ_2/L , noting always that we are in the regime of $\ell_1 \ll L$.

The main result of this calculation is that there are two distinct regimes of conductance quantization: (1) when $L_V \gg \ell_1$, $G_{S_1 D_3}$ is always quantized at $(1/3)e^2/h$ (up to exponentially small corrections in L/ℓ_1), regardless of the values of α or ℓ_2/L , and (2) when $L_V < \ell_1$ [see Fig. 6(a)] [35]. In the regime (2), we identify three main points of relevant behavior: (a) the region in parameter space where $\alpha \ll 1$, (b) a cross-over region

where $\alpha \sim 1$, and (c) where $\alpha \gg 1$. The conductance for these different regimes are shown in Fig. 6(a). To understand these conductance results, we transform into the charge/neutral mode basis, in analogy with the low temperature regime fixed points of Ref. [5]. In the $\alpha \ll 1$ regime, we note that this corresponds to the incoherent analogue of the intermediate fixed point where the tunneling between the outer-most mode and the inner three modes is ignored, and there are two co-propagating 1/3-charge modes which carry the current, which give $G_{S_1D_2} = G_{S_1D_3} = (1/3)e^2/h$ [see Fig. 6(b)]; deviations from the quantized value in the $\alpha \ll 1$ regime characterize the deviation from the intermediate fixed point. In the $\alpha \rightarrow \infty$ limit, the corresponding edge structure is that of a $\nu = 1/3$ low-density constriction where the counter-propagating 1/3-charge modes localize each other, counter-propagating 2/3 and neutral modes remain (KFP fixed point) [see Fig. 6(c)]. In this case, by using the results from a calculation of the counter-propagating 2/3 – 1/3 line junction (the calculation is straightforward and we omit it here), we see that the conductance $G_{S_1D_3} = (1/3)e^2/h$ when $L_V \gg \ell_1$, (with vanishingly small corrections as a function of L_V/ℓ_1), and vanishes for $\ell_1 \gg L_V$ (with vanishingly small corrections as a function of L_V/ℓ_1). In between these two limits, there is some continuous change between the two fixed point pictures, with a change of inflection in the conductance around the point $\alpha \sim 1$ from concave to convex, which is the transition point from g_1 processes being the strongest to g_2 processes being the strongest. We emphasize that the conductance behavior as a function of α is conceptually simpler in the charge/neutral mode picture than in the bare mode picture, and reproduces the results of our numerical calculations in the $\alpha \ll 1$ and $\alpha \rightarrow \infty$ limits.

Heat transport

Applying boundary conditions for the heat transport equations in the single QPC, there are again 22 equations in 22 unknowns, corresponding to the different segments of the QPC (see Appendix D). From this, we calculate numerically the conductances $K_{S_1D_2}, K_{S_1D_3}, K_{S_1D_4}$, and the conductance associated with current backscattered to contact A , namely K_{back} . The total injected current contributes a thermal conductance of $(4T_0)\pi^2k^2/6h$, so energy conservation dictates the following condition:

$$K_{S_1D_2} + K_{S_1D_3} + K_{S_1D_4} + K_{\text{back}} = \frac{\pi^2k^2}{6h}4T_0 \quad (43)$$

Results

For the QPC with the outermost channel transmitted, we expect now that the relevant length scales will be $\bar{\ell}_1, \bar{\ell}_2, L$ and L_V , and we can look at how the conductances vary as function of these parameters. We see several features:

- We see a power law in L in the conductances $K_{S_1D_2}, K_{S_1D_3}$, as we would naively expect from our previous analysis of heat transport in different geometries [see Fig. 7(a)]. However, this behavior only onsets once the condition $\bar{\ell}_1, \bar{\ell}_2 \ll L$ is satisfied, which is the condition for full equilibration. In the regime where $\bar{\ell}_1 \ll L < \bar{\ell}_2$, there is some non-trivial behavior where heat transport is non-vanishing, with a peak in the backscattered heat current appearing around $L \sim \bar{\ell}_2$, which indicates a change in transport from that with a non-equilibrated outermost edge to that with an equilibrated outermost edge. Additionally, we note that in the regime $\bar{\ell}_2 > L$, the deviations which $K_{S_1D_2}, K_{S_1D_3}$ and $K_{S_1D_4}$ have from each other drastically decrease as α increases.

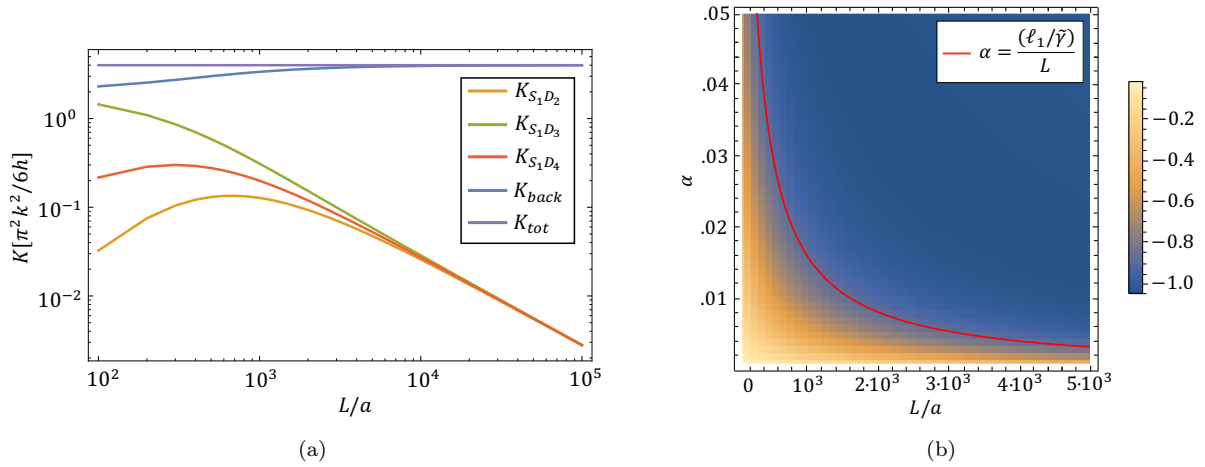


Figure 7: (a) Log-log plot of the thermal conductances $K_{S_1 D_2}, K_{S_1 D_3}, K_{S_1 D_4}, K_{back}$ in the single QPC as a function of L for $\alpha = .03, \ell_1 = 10a, L_V = 0a$, and $L = 10^2 a - 10^5 a$. We note that there is a marked change in the behavior of the conductance curves around $L \sim \bar{\ell}_2 \sim 560a$, beyond which the power law in L emerges; this is an indication of equilibration between edge modes. (b) Plot of the derivative $d(\ln(K_{S_1 D_3}))/d(\ln(L))$, which characterizes the onset of the power law, as a function of L and α for $L = 0 - 5000a$. We see that the onset of $1/L$ behavior for $K_{S_1 D_3}$ occurs when $\bar{\ell}_2 \lesssim L$, which happens when $\alpha \gtrsim \frac{(\ell_1/\tilde{\gamma})}{L}$. We overlay the curve $\alpha = \frac{(\ell_1/\tilde{\gamma})}{L}$, which matches qualitatively with the onset of $1/L$ behavior.

- Additionally, we note that the onset of the $1/L$ behavior is robust with changes in α , as can be seen in Fig. 7(b).
- The dependence of $K_{S_1D_2}$, $K_{S_1D_3}$ and $K_{S_1D_4}$ on L_V does not affect the onset of the power law in L . However, it does affect the relative magnitudes of $K_{S_1D_2}$, $K_{S_1D_3}$, $K_{S_1D_4}$, as we will describe in the following discussion below.

It is informative to compare these results with those of the MacDonald picture. In the MacDonald picture, the total injected heat current contributes a thermal conductance of $(2T_0)\pi^2k^2/6h$, so energy conservation dictates the following condition:

$$K_{S_1D_2} + K_{S_1D_3} + K_{S_1D_4} + K_{\text{back}} = \frac{\pi^2k^2}{6h}2T_0 \quad (44)$$

In the MacDonald picture, we obtain the following thermal conductances for the single QPC:

$$\begin{aligned} K_{S_1D_2} &= \frac{2L^2\bar{\ell}}{(2L + \bar{\ell})(2L^2 + 2L\bar{\ell} + \bar{\ell}^2)} \frac{\pi^2k^2}{6h} T_0 \\ K_{S_1D_3} &= \frac{2\bar{\ell}(L + \bar{\ell})^2}{(2L + \bar{\ell})(2L^2 + 2L\bar{\ell} + \bar{\ell}^2)} \frac{\pi^2k^2}{6h} T_0 \\ K_{S_1D_4} &= \frac{2L\bar{\ell}(L + \bar{\ell})}{(2L + \bar{\ell})(2L^2 + 2L\bar{\ell} + \bar{\ell}^2)} \frac{\pi^2k^2}{6h} T_0 \\ K_{\text{back}} &= \frac{2L(4L^2 + 3L\bar{\ell} + \bar{\ell}^2)}{(2L + \bar{\ell})(2L^2 + 2L\bar{\ell} + \bar{\ell}^2)} \frac{\pi^2k^2}{6h} T_0 \end{aligned} \quad (45)$$

We can now ask if there is a way to distinguish between the MacDonald and WMG edge structures from these thermal conductance measurements. From Eq. (46), we see that the condition that $K_{S_1D_3} > K_{S_1D_4} > K_{S_1D_2}$ always holds for the MacDonald case. Comparing to the WMG case, if we set $\bar{\ell}_2 = \bar{\ell}$ and look at the regime where $\bar{\ell}_1 \ll \bar{\ell}_2$, we find that the thermal conductances of the WMG and MacDonald edges are nearly identical; more generally, for the WMG case we find that in the regime where $\bar{\ell}_1 \ll \bar{\ell}_2$, the condition $K_{S_1D_3} > K_{S_1D_4} > K_{S_1D_2}$ holds as we vary the system size from a non-equilibrated regime ($L < \bar{\ell}_1, \bar{\ell}_2$) to a fully equilibrated one ($L \gg \bar{\ell}_1, \bar{\ell}_2$). Thus in this regime, there is no robust signature in the thermal conductance that would allow us to distinguish between the two edge structures. However, in the regime where $\bar{\ell}_1 \gg \bar{\ell}_2, \ell_1 \gg L_V$, the following condition is met: $K_{S_1D_2} > K_{S_1D_3} > K_{S_1D_4}$, differing from the MacDonald case. This condition holds as we vary the system size from a non-equilibrated regime ($L < \bar{\ell}_1, \bar{\ell}_2$) to a fully equilibrated one ($L \gg \bar{\ell}_1, \bar{\ell}_2$), and is therefore a robust signature which distinguishes the WMG picture from the MacDonald picture. However, we note that the inequality $K_{S_1D_2} > K_{S_1D_3} > K_{S_1D_4}$ returns to $K_{S_1D_3} > K_{S_1D_4} > K_{S_1D_2}$ as we increase $L_V \gtrsim \bar{\ell}_1$. Thus, the WMG edge is only distinguishable in a robust manner when the system is in the limit of small constriction width, i.e. $\ell_1 \gg L_V$, with the additional condition that $\bar{\ell}_1 \gg \bar{\ell}_2$.

3.3. Transport in a double QPC

Electrical transport in the winding case

In the case of electrical transport in a double QPC with circulating edge states in between the two QPCs, we have the same sets of equations as before, but now with 36 boundary conditions to match (see Appendix D). We

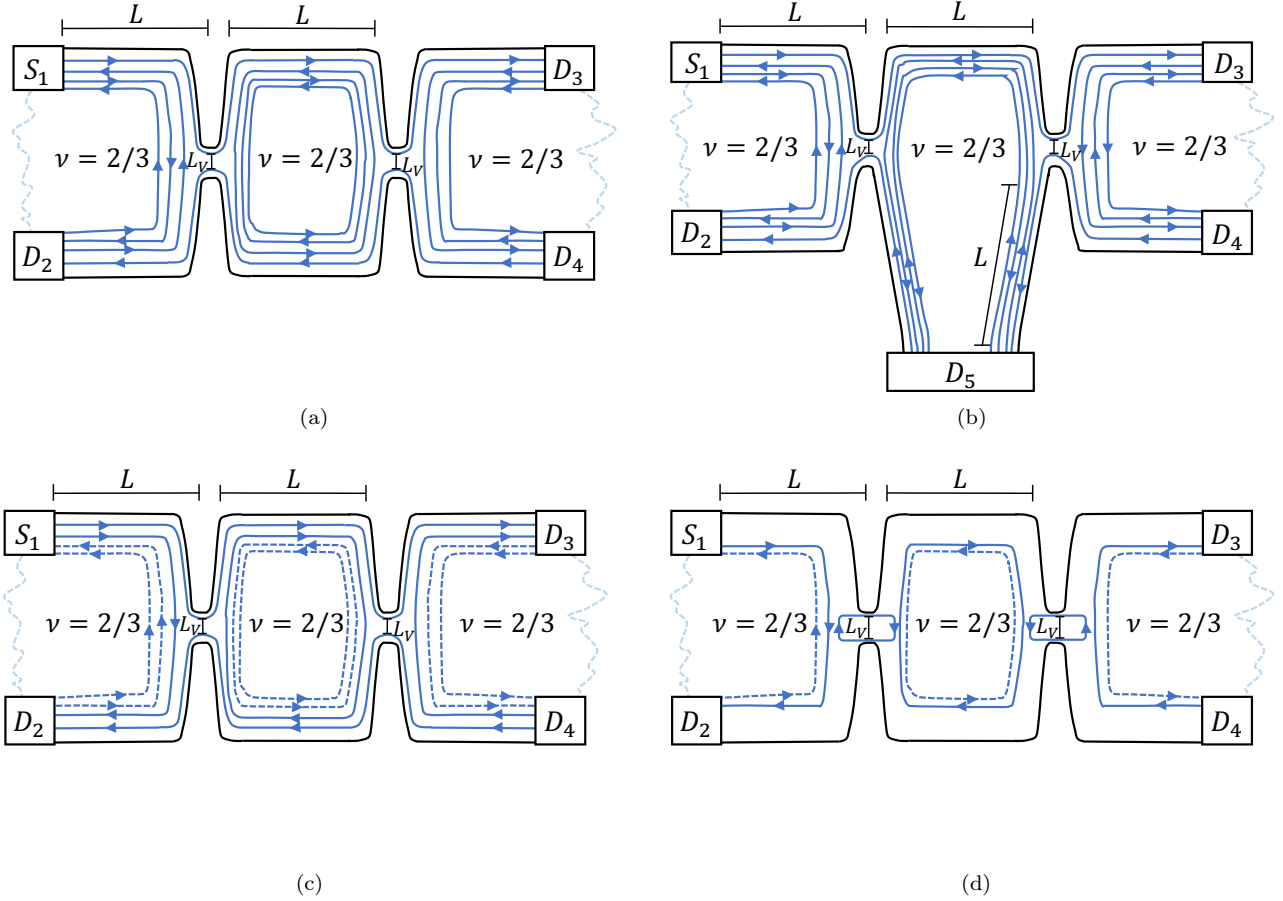


Figure 8: (a) Bare modes of the double QPC in the “winding” geometry. The width of the constriction is L_V , the length of an arm of a QPC is L , and the circumference of the winding edge states in between the two QPCs is $2L$. There are additional edge structures for this geometry, in analogy with (b) – (d) of this figure. (b) Bare modes of the double QPC in the “no-winding” geometry. The length of the path that the edge states travel between the two QPCs is $3L$ (c) Incoherent analogue of the WMG intermediate fixed point in the “winding” geometry (the decay of the neutral modes is not shown). This picture reproduces the same conductance results as our model in regime with $\ell_2 > L$. (d) Incoherent analogue of the KFP fixed point in the “winding” geometry, with $\nu = 1/3$ QH droplets in the constrictions (the decay of the neutral modes is not shown). This picture reproduces the same conductance results as our model in the limit that $\alpha \rightarrow \infty$.

refer to this geometry as the “winding” case [see Fig. 8(a)]. As in the case of electrical transport in the single QPC, from the numerical calculations we see two main regimes of behavior for the conductance $G_{S_1 D_3}$: (1) for $\ell_1 < L_V$, in the case where $\alpha \sim 0$ (the outermost edge is decoupled), the conductance is quantized at $(1/3)e^2/h$, and drops down from this value as α is increased, dropping to $(2/9)e^2/h$ as $\alpha \sim \ell_1/L \rightarrow \ell_2 \sim L$. Beyond this point, α is quantized at $(2/9)e^2/h$. (2) In the case $\ell_1 \gg L_V$, we see the same behavior of $G_{S_1 D_3}$ up to $\ell_2 \sim L$, but beyond this point, the conductance decreases with α as in the single QPC case, approaching 0 as $\alpha \rightarrow \infty$ [see Figs. 9(a, b)]. Again, we can explain these behaviors in the charge/neutral mode basis in the limits of $\alpha \ll 1$ and $\alpha \rightarrow \infty$. In the $\alpha \ll 1$ case, where the edge structure is the incoherent analogue of the intermediate fixed point [see Fig. 8(c)], we can see the transition from $G_{S_1 D_3} = (1/3)e^2/h$ to $G_{S_1 D_3} = (2/9)e^2/h$ as a function of ℓ_2/L [see Figs. 9(a, b)]; in the case of $L \ll \ell_2$, nearly all of the injected current on the uppermost mode is carried to drain D_3 , and $G_{S_1 D_3} \sim (1/3)e^2/h$ with deviations growing as ℓ_2 decreases. Near $\ell_2 \sim L$, assuming full equilibration between the two charge modes in the island between the QPCs, a short calculation yields $G_{S_1 D_3} = (2/9)e^2/h$. In the $\alpha \rightarrow \infty$ case, we again have the incoherent analogue of the KFP edge structure with $1/3$ density constrictions at the QPCs, as in Fig. 8(d). Using this effective edge structure, and assuming equilibration between counter-propagating charge modes (again using the results from the counter-propagating $2/3 - 1/3$ line junction), one can easily calculate $G_{S_1 D_3} = (2/9)e^2/h$. Thus, as α is varied, we imagine that the picture of the edge states is varied from that of the intermediate fixed point edge structure to the KFP edge structure, just as in the case of the single QPC. Additionally, we see that in the case (2), we see the slow decay in conductance as a function of α being controlled by the competition of g_1 and g_2 , as was seen in the single QPC case. Thus around $\alpha \sim 1$, there is a change of inflection in the conductance curve as a function of α from concave to convex, as in the single QPC case. In the limit of an extremely narrow constriction with $L_V \rightarrow 0$, the conductances $G_{S_1 D_3}$ ($G_{S_1 D_2}$) do not saturate at the above described bounds, but instead monotonically decrease (increase) as in Figs. 9(a, b), eventually reaching the values 0 ($(2/3)e^2/h$) in the $\alpha \rightarrow \infty$ limit.

Electrical transport in the no-winding case

In the presence of an Ohmic contact between the two QPCs, edge states can no longer circulate in between the two QPCs. We refer to this geometry as the “no-winding” case [see Fig. 8(b)]. The results of the no-winding case are analogous to the winding case, with the difference that $G_{S_1 D_3}$ changes from $(1/3)e^2/h$ for $L \ll \ell_2$ to $(1/6)e^2/h$ for $L \geq \ell_2$ in both the $\ell_1 < L_V$ and the $\ell_1 > L_V$ regimes (once again, in the regime where $\ell_1 > L_V$, as ℓ_2 decreases beyond $\ell_2 \sim L$, $G_{S_1 D_3}$ decreases, vanishing as $\alpha \rightarrow \infty$ [see Fig. 8(c), 8(d) for renormalized edges]). We note that similar results were seen in a recent experiment [21]. In this experiment, Sabo et al. [21] tested two devices, one with a small separation between the QPCs ($\sim 4\mu m$) and one with a large separation between the two QPCs ($\sim 9\mu m$), and the conductance $G_{S_1 D_3}$ changed from $(1/3)e^2/h$ to $(1/6)e^2/h$, which is consistent with the transition from $L \ll \ell_2$ to $L \geq \ell_2$ in our model.

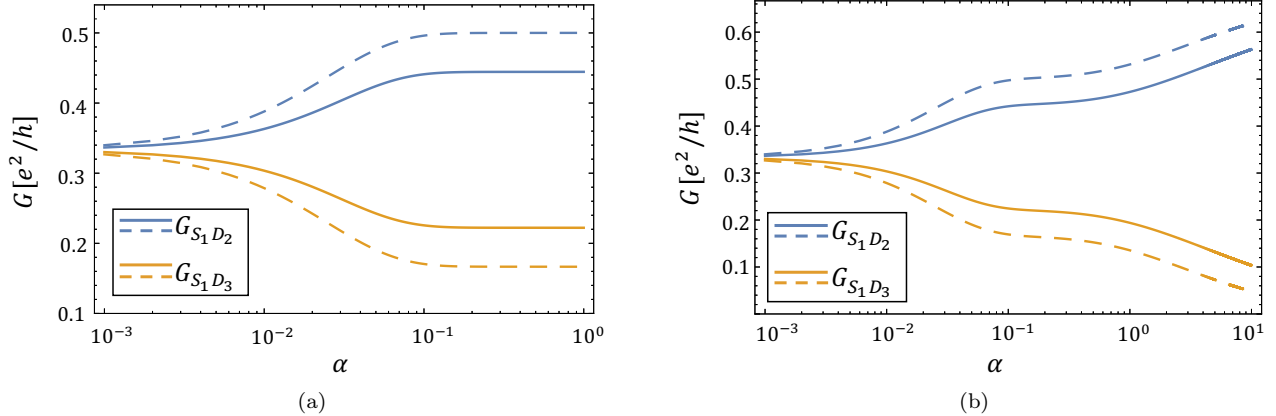


Figure 9: (a) Log-linear conductance plot of the conductances $G_{S_1 D_2}, G_{S_1 D_3}$ as a function of α for $L = 100a, L_V = 10a, \ell_1 = 5a$; the dashed lines correspond to the “no-winding” geometry, and the solid lines correspond to the “winding” geometry. (b) Log-linear conductance plot of the conductances $G_{S_1 D_2}, G_{S_1 D_3}$ as a function of α in the limit of a narrow constriction with, $L = 100a, L_V = 0, \ell_1 = 5a$; the convention is the same as in 9(a).

4. Summary and Discussion

4.1. Summary

In this work, we study transport along the QH edge for the $\nu_{\text{bulk}} = 2/3$ FQH state, where impurity mediated tunneling between adjacent modes induces equilibration. We assume that we are in the incoherent regime, where subsequent tunneling events are incoherent with each other, allowing us to ignore phase interference effects. Our model is a discrete model consisting of counter-propagating modes linked by “tunneling bridges” [see Fig. 2(a)]; the particular form of the tunneling current can be calculated from the LL theory using the Keldysh formalism, as discussed in Appendix B. Using this form for the tunneling current and the local constitutive relations for each mode (e.g. Eq. (1)), we then impose current and energy conservation for each channel at each tunneling bridge, and go to the continuum limit by taking the smallest scale of variation as $ia \rightarrow x$ and taking the number of tunneling bridges $n \rightarrow \infty$. We finally apply boundary conditions from ideal contacts to obtain temperature and voltage profiles, and thermal and electrical conductances.

Within this scheme, we study two relevant models for the edge structure at $\nu_{\text{bulk}} = 2/3$ (MacDonald and WMG). The MacDonald model (which should be relevant for a sharply-defined confining potential), consists of two counter-propagating modes, a $\delta\nu = +1$ channel and a counter-propagating $\delta\nu = -1/3$ channel. The WMG model (which is relevant for a shallow confining potential), consists of four channels, which are (counting from the bulk to the edge): a $\delta\nu = +1/3$ mode, a $\delta\nu = -1$ mode, a $\delta\nu = +1/3$ mode, and a final $\delta\nu = -1/3$ mode. In the MacDonald picture, we consider only electron tunneling between channels, and in the WMG picture, we consider the most relevant (in the RG sense) electron and two-electron tunneling operators between the inner three modes, and $1/3$ -charge tunneling between the outermost mode and the adjacent mode.

We now describe the main results of these calculations:

- **MacDonald edge:** For the MacDonald edge, we obtain quantized conductances with corrections. In the line junction, the thermal conductance of the transmitted channel $K \sim (\pi^2 k^2 T_0 / 3h) (\bar{\ell} / L)$ (vanishing thermal conductance with finite diffusive conductivity), while the corresponding electrical conductance results reproduce the quantization, but with *exponentially* small corrections, i.e. $G \sim (2e^2 / 3h) \left(1 + e^{-\frac{2\bar{\ell}}{\ell}} / 3\right)$. If we compare with the typical case of counter-propagating $\delta\nu = +1, -1$ modes, which corresponds to a quantum wire, we obtain vanishing electrical conductance with diffusive ($\sim \ell / L$) conductivity corrections. Following KFP and switching to the charge/neutral basis, we see that the neutral mode decays exponentially from the drain as $\sim e^{-\frac{2\bar{\ell}}{\ell}}$, and is proportional to the tunneling current; thus, the decay of the neutral mode directly reflects the equilibration of the channels. This effect is also seen in the voltage induced temperature profiles, where thermal equilibration occurs between the $\delta\nu = +1$ and $\delta\nu = -1/3$ modes within a scattering length $\sim \ell$ of the drain, and as a consequence generates heat near the drain. Despite such heating effects, we find that the thermoelectric response coefficients are identically zero; this is a reflection of the particle-hole symmetry of the linearized dispersion in the LL model [42].
- **WMG:** For the WMG edge structure, we numerically examine electrical and heat transport in a single-QPC geometry, and electrical transport in two different double-QPC geometries (the geometries are given in Figs. 8(a) and 8(b), respectively). In this model, we have two competing scattering lengths ℓ_1 and ℓ_2 , which are associated with tunneling between the inner-three modes and the outer-mode tunneling, respectively; the competition between these types of tunneling is controlled by the parameter $\alpha \equiv \ell_1 / \ell_2$. Additionally, the QPC is characterized by two length scales, L_V, L , which are the width of the QPC and the length of an arm of the QPC, respectively. We see that the conductance results can be replicated by a simplified analysis in the charge/neutral mode basis. For electrical transport in the single-QPC geometry, we find that the conductance from the source to drain $G_{S_1 D_3}$ at $\alpha \ll 1$ matches well to the intermediate fixed point edge structure, while the $\alpha \rightarrow \infty$ behavior matches the KFP edge structure, with some crossover behavior; in this setup, backscattering is strongly enhanced for $\ell_1 > L_V$. In the double QPC geometries, we obtain transitions from $(1/3)e^2/h$ to quantized conductances of $(2/9)e^2/h$ and $(1/6)e^2/h$ in the “winding” and “no-winding” geometries, respectively [see Fig. 9], with similarly enhanced backscattering for $\ell_1 > L_V$; again, all of the relevant features can be reproduced by the corresponding fixed point edge structures in the $\alpha \ll 1$ and $\alpha \rightarrow \infty$ regimes, with some continuous transition between them [see Figs. 8(c, d)]. Finally, heat transport in the single QPC has $\sim 1/L$ decay when the appropriate scattering lengths $\bar{\ell}_1, \bar{\ell}_2 \ll L$, with some non-universal behavior occurring for $\bar{\ell}_1 \ll L \lesssim \bar{\ell}_2$ [see Figs. 7(a, b)]. This behavior is nearly identical to the results of the MacDonald model. However, it is possible to distinguish between the two models in the regime where $\bar{\ell}_1 \gg \bar{\ell}_2, \ell_1 \gg L_V$ by examining the thermal conductances at the three drains D_2, D_3, D_4 : in the MacDonald model we find that the thermal conductances always obey the inequality $K_{S_1 D_3} > K_{S_1 D_4} > K_{S_1 D_2}$, whereas in this regime the WMG model follows $K_{S_1 D_2} > K_{S_1 D_3} > K_{S_1 D_4}$.

4.2. Discussion

We have seen from our incoherent, disordered transport model that we can gain more insight into the process of equilibration between counter-propagating modes in the $\nu_{\text{bulk}} = 2/3$ FQH state. In particular, we see that equilibration is essential for conductance quantization, and that conductance quantization is achieved when the system size is much larger than the appropriate scattering length, i.e. $\ell \ll L$. In the case where there are multiple scattering lengths and system size parameters (as in the case of the single and double-QPC configurations with the outermost channel transmitted), we have found that a variety of conductance results can be obtained, and that the analysis can be simplified by switching to the charge/neutral mode picture. Here we find that our model

reproduces the fixed points of the WMG model in the incoherent setting, with some crossover behavior. For the thermal transport results, we can similarly see how equilibration plays a role in the conductance quantization, as we obtain that the thermal conductance vanishes as $\sim \bar{\ell}/L$ in the regime that $\bar{\ell} \ll L$ in the case of two counter-propagating modes (also as $\sim 1/L$ with the condition that $\bar{\ell}_1, \bar{\ell}_2 \ll L$ in WMG case). Our model also admits local voltage and temperature information on the edge, which shows how the equilibration process takes place.

Additionally, our calculation of the electrical conductance $G_{S_1 D_3}$ in the two QPC geometry matches the experimental conductance crossover from $(1/3)e^2/h$ to $(1/6)e^2/h$ as a function of the separation between the QPCs [21]; in our model, this can be understood simply as equilibration between an incoming fully-biased mode and a grounded mode. This crossover behavior does not occur in the simpler MacDonald model, and thus provides evidence for validity of the WMG model. Also, while recent experimental progress with heat transport in the fractional regime has been achieved in the experiments of Banerjee et al. [32, 37], our predictions require more subtle experiments which can see how thermal conductance scales with the system size L .

However, there are some potential caveats concerning the results of our calculations. The local information of the temperature and voltage profiles is not easily accessible to experiment in the typical GaAs/AlGaAs interface. There has been some progress in measuring temperature locally using quantum dots [30, 43, 44, 45], however this method is only applicable at single points along the edge, and is not practical for measuring continually along the edge. Additionally, on the model level, the temperature dependence of the tunneling coefficients g was ignored in our calculation, and the electrical and energy tunneling currents were derived by assuming certain constraints about the temperature and voltage biases; these constraints are discussed in Appendix C.

5. Acknowledgments

We thank Igor Gornyi, Alexander Mirlin, Dmitri Polyakov, Ivan Protopopov, Yonathan Cohen, Wenmin Yang, and Moty Heiblum for helpful discussions. We acknowledge financial support from DFG Grant No. RO 2247/8-1, ISF Grant No. 1349/14, CRC 183 of the DFG, and the Italia-Israel Collaborative Laboratory QUANTRA.

Appendix A. Some bosonization details

The action for the bosonic edge fields is of the form:

$$S = \frac{\hbar}{4\pi} \int dx dt \sum_{ij} (K_{ij} \partial_t \phi_i \partial_x \phi_j - V_{ij} \partial_x \phi_i \partial_x \phi_j), \quad (\text{A.1})$$

where K_{ij} an integer-valued symmetric matrix and V_{ij} is a positive definite matrix, with $K_{ij} = \text{diag}[3, -3, 1, -3]$ in our case. The definition of the current is [25]

$$I_i = K_{il}^{-1} V_{lj} \rho_j, \quad (\text{A.2})$$

with $\rho_j = -e(1/2\pi) \partial_x \phi_j$ the charge density of the j^{th} channel. The topological order of the state is fully characterized by the matrix K and the charge vector \mathbf{t} ; we work in the so-called ‘‘symmetric basis’’, where $\mathbf{t} = (1, 1, 1, 1)^T$ and $K = \text{diag}[3, -3, 1, -3]$. Additionally, the filling factor is given by $\nu = \sum_{ij} t_i K_{ij}^{-1} t_j$ and the filling factor discontinuities are given by $\delta\nu_i = \sum_j t_i K_{ij}^{-1} t_j$; in the bare-mode basis, the filling factor

discontinuities are $\delta\nu_1 = +1/3, \delta\nu_2 = -1/3, \delta\nu_3 = +1, \delta\nu_4 = -1/3$, as noted in Fig. 1(b). The creation operator is of the form:

$$\hat{O}(x) = e^{i\sum_j n_j \phi_j(x)}, \quad (\text{A.3})$$

which creates an excitation at point x with charge $Q = (-e)\sum_{ij} n_i K_{ij}^{-1} t_j$. From these definitions, we can see that the scattering vectors defined by Eq. (27) produce no net charge as required, and that neutral modes should satisfy the conditions $Q = 0$ and $\delta\nu = 0$. Under a change of basis, the above quantities transform as:

$$\begin{aligned} K_{ij} &\rightarrow \tilde{K}_{ij} = U_{\alpha i} K_{\alpha\beta} U_{\beta j} \\ V_{ij} &\rightarrow \tilde{V}_{ij} = U_{\alpha i} K_{\alpha\beta} U_{\beta j} \\ t_i &\rightarrow \tilde{t}_i = U_{ji} t_j \\ n_i &\rightarrow \tilde{n}_i = U_{ji} n_j \\ \phi_i &\rightarrow \tilde{\phi}_i = U_{ij}^{-1} \phi_j \end{aligned} \quad (\text{A.4})$$

We can transform the fields ϕ_i into a new basis $\tilde{\phi}_i$. The transformations are defined such that the action remains invariant:

$$\tilde{S} = \frac{\hbar}{4\pi} \int dx dt \sum_{ij} (\tilde{K}_{ij} \partial_t \tilde{\phi}_i \partial_x \tilde{\phi}_j - \tilde{V}_{ij} \partial_x \tilde{\phi}_i \partial_x \tilde{\phi}_j), \quad (\text{A.5})$$

with $\tilde{K}_{ij} \equiv U_{\alpha i} K_{\alpha\beta} U_{j\beta}$, $\tilde{V}_{ij} \equiv U_{\delta i} V_{\delta\gamma} U_{j\gamma}$. We see that the current in the new basis is of the form:

$$\begin{aligned} \tilde{I}_i &= (\tilde{K}^{-1})_{il} \tilde{V}_{lj} \tilde{\rho}_j = \left[(U^{-1})_{i\alpha} (K^{-1})_{\alpha\beta} (U^{-1})_{l\beta} \right] [U_{\gamma l} V_{\gamma\delta} U_{\delta j}] \left[(U^{-1})_{j\omega} \rho_\omega \right] \\ &= (U^{-1})_{i\alpha} (K^{-1})_{\alpha\beta} V_{\beta\omega} \rho_\omega = (U^{-1})_{i\alpha} I_\alpha \end{aligned} \quad (\text{A.6})$$

We see that the current transforms in the same manner as the fields ϕ_i .

Additionally, we note that in the absence of tunneling, we assume a local current conservation condition even in the presence of local electric fields $E_{x,i} = -\partial_x V_i(x)$. For the discussion of the validity of this point, we refer the reader to the section titled **Bulk currents** in Ref. [25].

Appendix B. Calculation of tunneling currents

In this Appendix, we derive electrical tunneling current (Eq. (3)) and energy tunneling currents (Eq. (39)) between counter-propagating $\delta\nu_1 = +1$ and $\delta\nu_\nu = -\nu = -1/(2m+1)$ modes for $m \in \mathbb{Z}^+$, or $\delta\nu_1 = +\nu$ and $\delta\nu_2 = -\nu$ modes at a single tunneling bridge $x = x_{\text{tun}}$ [see Fig. 2(a)]. For the electric currents, we follow the similar scheme to Ref. [46]. We first consider the case of the counter-propagating $\delta\nu_1 = +1$ and $\delta\nu_\nu = -\nu$ modes. We assume that each mode is connected to each "reservoir" with electro-chemical potential $\mu_{1(\nu)} = \mu_0 + eV_{1(\nu)}$ and temperature $T_{1(\nu)}$. The total Hamiltonian is written as $H = H_0 + H_V + H_\tau$: H_0 is the Hamiltonian for the edge modes as

$$H_0 = \frac{\hbar}{4\pi} \int [v_1 (\partial_x \phi_1)^2 + \frac{v_\nu}{\nu} (\partial_x \phi_\nu)^2] dx. \quad (\text{B.1})$$

Here $\phi_{i=1,\nu}$ is bosonic field describing edge mode i , and velocities v_1 and v_ν reflect the interaction within each mode. We assume that the interaction between the modes is zero for simplicity. The Hamiltonian H_τ describing electron tunneling between the modes at $x = x_{\text{tun}}$ is written as

$$H_\tau = \sum_{\epsilon=\pm} [\Gamma_0 \Psi_1^\dagger(x_{\text{tun}}) \Psi_\nu(x_{\text{tun}})]^\epsilon = \frac{1}{2\pi b} (\Gamma_0 e^{-i(\phi_1(x_{\text{tun}}) + \phi_\nu(x_{\text{tun}})/\nu)} + \text{H.c.}), \quad \text{with} \begin{cases} [\Gamma_0 \Psi_1^\dagger \Psi_\nu]^+ &= \Gamma_0 \Psi_1^\dagger \Psi_\nu, \\ [\Gamma_0 \Psi_1^\dagger \Psi_\nu]^- &= \Gamma_0^* \Psi_\nu^\dagger \Psi_1, \end{cases} \quad (\text{B.2})$$

where Γ_0 is tunneling amplitude, a field operator $\Psi_i^\dagger(x) = \exp[-i\phi_i(x)/\delta\nu_i]/\sqrt{2\pi b}$ creates an electron at position x on mode $i = 1, \nu$ and b is the smallest length scale corresponding to the ultraviolet spatial cutoff. Coupling each edge mode to each effective reservoir leads to

$$H_V = -\frac{1}{2\pi} \sum_{i=1,\nu} \int \mu_i \partial_x \phi_i dx. \quad (\text{B.3})$$

The tunneling current operator I_τ is derived from the Heisenberg equation of motion as

$$I_\tau(t) = \frac{d}{dt} \left(\frac{e}{2\pi} \int dx \partial_x \phi_1 \right) = -\frac{ie}{\hbar} \sum_{\epsilon=\pm} \epsilon [\Gamma_0 \Psi_1^\dagger(x_{\text{tun}}) \Psi_\nu(x_{\text{tun}})]^\epsilon, \quad (\text{B.4})$$

where we employed the commutation relation of $[\phi_i(x), \phi_i(x')] = i\pi\delta\nu_i \text{sgn}(x - x')$. The tunneling Hamiltonian $H_{\tau, H_0 + H_V}$ and the tunneling current operator $I_{\tau, H_0 + H_V}$ in the interaction picture with respect to $H_0 + H_V$ are written in terms of operators in the interaction picture with respect to H_0 (denoted as subscript H_0) as

$$\begin{aligned} H_{\tau, H_0 + H_V}(t) &= \sum_{\epsilon=\pm} e^{-i\epsilon e(V_1 - V_\nu)t/\hbar} [\Gamma_0 \Psi_{1, H_0}^\dagger(x_{\text{tun}}, t) \Psi_{\nu, H_0}(x_{\text{tun}}, t)]^\epsilon, \\ I_{\tau, H_0 + H_V}(t) &= -\frac{ie}{\hbar} \sum_{\epsilon=\pm} \epsilon e^{-i\epsilon e(V_1 - V_\nu)t/\hbar} [\Gamma_0 \Psi_{1, H_0}^\dagger(x_{\text{tun}}, t) \Psi_{\nu, H_0}(x_{\text{tun}}, t)]^\epsilon. \end{aligned} \quad (\text{B.5})$$

In the Keldysh formalism, the tunneling current is written as

$$\langle I_\tau(t) \rangle = \frac{1}{2} \sum_{\eta=\pm 1} \langle T_C I_{\tau, H_0 + H_V}(t^\eta) e^{-\frac{i}{\hbar} \int_C dt_1 H_{\tau, H_0 + H_V}(t_1^{\eta_1})} \rangle, \quad (\text{B.6})$$

where t^η denotes time t on a upper (lower) branch $\eta = \pm 1$ of Keldysh contour C and is ordered in Keldysh ordering: Keldysh ordering is defined as $t_1^- > t_2^+$ for all t_1 and t_2 , $t_1^+ > t_2^+$ for $t_1 > t_2$, and $t_1^- > t_2^-$ for $t_1 < t_2$. Keldysh ordering operator T_C arranges operators in a sequence of their time argument's Keldysh ordering. Making use of Eq. (B.5), Eq. (B.6) in the second order in Γ_0 becomes

$$\begin{aligned} \langle I_\tau(t) \rangle &\simeq \frac{e|\Gamma_0|^2}{2\hbar^2} \sum_{\eta, \eta_1=\pm 1} \sum_{\epsilon=\pm} \epsilon \eta_1 \int_{-\infty}^{\infty} dt_1 e^{i\epsilon e(V_1 - V_\nu)(t - t_1)/\hbar} \\ &\times \langle T_C [\Psi_{1, H_0}^\dagger(x_{\text{tun}}, t^\eta) \Psi_{\nu, H_0}(x_{\text{tun}}, t^\eta)]^\epsilon [\Psi_{1, H_0}^\dagger(x_{\text{tun}}, t_1^{\eta_1}) \Psi_{\nu, H_0}(x_{\text{tun}}, t_1^{\eta_1})]^{-\epsilon} \rangle, \\ &= \frac{ie|\Gamma_0|^2}{\hbar^2 b^2} \sum_{\eta, \eta_1=\pm 1} \eta_1 \int_{-\infty}^{\infty} dt_1 \left[\sin\left\{ \frac{e}{\hbar} (V_1 - V_\nu)(t - t_1) \right\} e^{G_1^{\eta_1}(t - t_1)} e^{G_\nu^{\eta_1}(t - t_1)/\nu^2} \right]. \end{aligned} \quad (\text{B.7})$$

Here we introduce the Keldysh Green's function of mode $\phi_{i=1,\nu}$, $G_i^{\eta_1\eta_2}(x, t_1 - t_2) = \langle T_C \phi_i(x, t_1^{\eta_1}) \phi_i(0, t_2^{\eta_2}) \rangle - \langle T_C \phi_i(0, t_1^{\eta_1}) \phi_i(0, t_2^{\eta_1}) \rangle$, which is calculated as

$$G_{i=1,\nu}^{\eta_1\eta_2}(x, t) = -|\delta\nu_i| \ln \left[\frac{\sin[\pi(b + i(v_i t \mp x)\chi_{\eta_1\eta_2}(t))/\hbar v_i \beta_i]}{\pi b/\hbar v_i \beta_i} \right], \quad (\text{B.8})$$

where $\beta_i \equiv 1/(k_B T_i)$ is the inverse temperature of mode $i = 1, \nu$, $-(+)$ represents chirality of mode $i = 1(\nu)$, and $\chi_{\eta_1\eta_2}(t) \equiv [(\eta_1 + \eta_2)/2] \text{sgn}(t) - (\eta_1 - \eta_2)/2$. Because $G_i^{\eta\eta}(t)$ is symmetric with respect to $t = 0$, $G_i^{\eta\eta}(t)$ contribution in Eq. (B.7) is zero, and then Eq. (B.7) becomes

$$\begin{aligned} \langle I_\tau(t) \rangle &= -\frac{ie|\Gamma_0|^2}{h^2 b^2} \sum_{\eta=\pm 1} \eta \int_{-\infty}^{\infty} dt' \sin\left(\frac{et'}{\hbar}(V_1 - V_\nu)\right) e^{G_1^{\eta-\eta}(t')} e^{G_\nu^{\eta-\eta}(t')/\nu^2}, \\ &= -\frac{ie|\Gamma_0|^2}{h^2 b^2} \sum_{\eta=\pm 1} \eta \int_{-\infty}^{\infty} dt' \sin\left(\frac{et'}{\hbar}(V_1 - V_\nu)\right) \left(\frac{\pi b/\hbar v_1 \beta_1}{\sin[\pi(b - i\eta v_1 t')/\hbar v_1 \beta_1]}\right) \left(\frac{\pi b/\hbar v_\nu \beta_\nu}{\sin[\pi(b - i\eta v_\nu t')/\hbar v_\nu \beta_\nu]}\right)^{1/\nu}. \end{aligned} \quad (\text{B.9})$$

When the change of variable $t' \rightarrow t' - ib\eta/v_\nu + i\eta\hbar\beta_\nu/2$ is performed, the integral becomes simplified as

$$\begin{aligned} \langle I_\tau(t) \rangle &= -\frac{ie|\Gamma_0|^2}{h^2 b^2} \sum_{\eta=\pm 1} \eta \int_{-\infty+ib\eta/v_\nu-i\eta\hbar\beta_\nu/2}^{\infty+ib\eta/v_\nu-i\eta\hbar\beta_\nu/2} dt' \sin\left[\frac{e(t' + i\eta\hbar\beta_\nu/2)}{\hbar}(V_1 - V_\nu)\right] \\ &\quad \times \left(\frac{\pi b/\hbar v_1 \beta_1}{\sin\left[\frac{\pi}{\hbar v_1 \beta_1}\left\{b\left(1 - \frac{v_1}{v_\nu}\right) - i\eta v_1 t' + \frac{\hbar\beta_\nu v_1}{2}\right\}\right]}\right) \left(\frac{\pi b/\hbar v_\nu \beta_\nu}{\sin\left(\frac{\pi}{2} - \frac{i\eta\pi t'}{\hbar\beta_\nu}\right)}\right)^{1/\nu} \\ &= -\frac{ie|\Gamma_0|^2}{h^2 b^2} \sum_{\eta=\pm 1} \eta \int_{-\infty}^{\infty} dt' \sin\left[\frac{e(V_1 - V_\nu)(t' + i\eta\hbar\beta_\nu/2)}{\hbar}\right] \left(\frac{\pi b/\hbar v_\nu \beta_\nu}{\cosh(\pi t'/\hbar\beta_\nu)}\right)^{1/\nu} \left(\frac{\pi b/\hbar v_1 \beta_1}{\sin\left(\frac{\pi\beta_\nu}{2\beta_1} - \frac{i\eta\pi t'}{\hbar\beta_1}\right)}\right). \end{aligned} \quad (\text{B.10})$$

In the second equality of Eq. (B.10), we changed the integral range back to $-\infty$ to ∞ because in the integrand of the first right hand side term of Eq. (B.10), there is no pole inside the rectangular contour with vertices $t' = \infty, -\infty, -\infty + ib\eta/v_\nu - i\eta\hbar\beta_\nu/2$, and $\infty + ib\eta/v_\nu - i\eta\hbar\beta_\nu/2$. under the condition of $\hbar v_\nu \beta_\nu > b$. In the limit of $|T_1 - T_\nu| \ll \bar{T} \equiv (T_1 + T_\nu)/2$, the leading term of Eq. (B.10) in $|T_1 - T_\nu|$ is obtained, replacing T_1 and T_ν by \bar{T} , as

$$\begin{aligned} \langle I_\tau(t) \rangle &\simeq \frac{2e|\Gamma_0|^2}{h^2 b^2} \sinh\left(\frac{e(V_1 - V_\nu)}{2k_B \bar{T}}\right) \int_{-\infty}^{\infty} dt' \cos\left(\frac{e(V_1 - V_\nu)t'}{\hbar}\right) \left(\frac{\pi b k_B \bar{T}/\hbar v_\nu}{\cosh(k_B \bar{T} \pi t'/\hbar)}\right)^{1/\nu} \left(\frac{\pi b k_B \bar{T}/\hbar v_1}{\cosh(k_B \bar{T} \pi t'/\hbar)}\right) \\ &= \frac{2e|\Gamma_0|^2}{h^2 b^2} \left(\frac{\pi b k_B \bar{T}}{\hbar v_\nu}\right)^{1/\nu} \left(\frac{\pi b k_B \bar{T}}{\hbar v_1}\right) \sinh\left(\frac{e(V_1 - V_\nu)}{2k_B \bar{T}}\right) \int_{-\infty}^{\infty} dt' \frac{\cos[e(V_1 - V_\nu)t'/\hbar]}{[\cosh(k_B \bar{T} \pi t'/\hbar)]^{1/\nu+1}} \\ &= \frac{2^{1+1/\nu} e|\Gamma_0|^2}{h^2 b v_1} \left(\frac{\pi b k_B \bar{T}}{\hbar v_\nu}\right)^{1/\nu} \sinh\left(\frac{e(V_1 - V_\nu)}{2k_B \bar{T}}\right) \frac{|\Gamma(\frac{1}{2} + \frac{1}{2\nu} + i\frac{e(V_1 - V_\nu)}{2\pi k_B \bar{T}})|^2}{\Gamma(1 + 1/\nu)}, \end{aligned} \quad (\text{B.11})$$

where $\Gamma(x)$ is a gamma function and we used the integral equality $\int_{-\infty}^{\infty} dt \cosh(2yt)/\cosh^{2x} t = 2^{2x-1} \Gamma(x+y)\Gamma(x-y)/\Gamma(2x)$ in the case of $\text{Re } x > |\text{Re } y|$ and $\text{Re } x > 0$. In the case of $e(V_1 - V_\nu) \ll k_B \bar{T}$, the tunneling

current is proportional to the voltage difference ($V_1 - V_\nu$) as

$$\langle I_\tau(t) \rangle = g_1 \frac{e^2}{h} (V_1 - V_\nu), \quad \text{where } g_1 = \frac{(2\pi)^{\frac{1}{\nu}-1} [\Gamma(\frac{1}{2} + \frac{1}{2\nu})]^2}{\Gamma(1 + \frac{1}{\nu})} \left(\frac{|\Gamma_0|^2 / b^2}{(\hbar v_1 / b) k_B \bar{T}} \right) \left(\frac{k_B \bar{T}}{(\hbar v_\nu / b)} \right)^{\frac{1}{\nu}}. \quad (\text{B.12})$$

Note that a dimensionless effective conductance g scales as $\bar{T}^{(1/\nu-1)}$. It proves Eq. (3) in the main text.

Let us do a similar calculation for the energy current J_τ in the same geometry as the above. The tunneling energy current is written as

$$J_\tau = -\frac{1}{2} \frac{d}{dt} (H_L - H_R) = \frac{i}{4} \sum_{\epsilon=\pm} \epsilon \left\{ (v_1 \partial_x \phi_1 |_{x=x_{\text{tun}}} + \frac{v_\nu}{\nu} \partial_x \phi_\nu |_{x=x_{\text{tun}}} - \frac{\mu_1 + \mu_\nu}{\hbar}), [\Gamma_0 \Psi_1^\dagger(x_{\text{tun}}) \Psi_\nu(x_{\text{tun}})]^\epsilon \right\}, \quad (\text{B.13})$$

where $\{A, B\} = AB + BA$ and we defined H_L and H_R as

$$H_L = \frac{\hbar v_1}{4\pi} \int (\partial_x \phi_1)^2 dx - \frac{1}{2\pi} \int \mu_1 \partial_x \phi_1 dx, \quad H_R = \frac{\hbar v_\nu}{4\pi\nu} \int (\partial_x \phi_\nu)^2 dx - \frac{1}{2\pi} \int \mu_\nu \partial_x \phi_\nu dx. \quad (\text{B.14})$$

The tunneling energy current operator $J_{\tau, H_0 + H_V}$ in the interaction picture with respect to $H_0 + H_V$ is related to operators in the interaction picture with respect to H_0 (denoted as subscript H_0) as

$$J_{\tau, H_0 + H_V} = \frac{i}{4} \sum_{\epsilon=\pm} \epsilon e^{-i\epsilon e(V_1 - V_\nu)t/\hbar} \left\{ (v_1 \partial_x \phi_{1, H_0} |_{x=x_{\text{tun}}} + \frac{v_\nu}{\nu} \partial_x \phi_{\nu, H_0} |_{x=x_{\text{tun}}} - \frac{\mu_1 + \mu_\nu}{\hbar}), [\Gamma_0 \Psi_{1, H_0}^\dagger(x_{\text{tun}}, t) \Psi_{\nu, H_0}(x_{\text{tun}}, t)]^\epsilon \right\}, \quad (\text{B.15})$$

In the Keldysh formalism, the tunneling energy current is written as

$$\langle J_\tau^E(t) \rangle = \frac{1}{2} \sum_{\eta=\pm 1} \langle T_C J_{\tau, H_0 + H_V}(t^\eta) e^{-\frac{i}{\hbar} \int_C dt_1 H_{\tau, H_0 + H_V}(t_1^{\eta_1})} \rangle. \quad (\text{B.16})$$

In the second order in Γ_0 , the tunneling energy current becomes

$$\begin{aligned} \langle J_\tau(t) \rangle &\simeq \frac{|\Gamma_0|^2}{8\hbar} \sum_{\eta, \eta_1=\pm 1} \sum_{\epsilon=\pm} \epsilon \eta_1 \int_{-\infty}^{\infty} dt_1 e^{-i\epsilon e(V_1 - V_\nu)(t-t_1)/\hbar} \langle T_C \left\{ (v_1 \partial_x \phi_{1, H_0} |_{x=x_{\text{tun}}} + \frac{v_\nu}{\nu} \partial_x \phi_{\nu, H_0} |_{x=x_{\text{tun}}} - \frac{\mu_1 + \mu_\nu}{\hbar}) \right. \\ &\quad \left. , [\Psi_{1, H_0}^\dagger(x_{\text{tun}}, t^\eta) \Psi_{\nu, H_0}(x_{\text{tun}}, t^\eta)]^\epsilon \right\} [\Psi_{1, H_0}^\dagger(x_{\text{tun}}, t_1^{\eta_1}) \Psi_{\nu, H_0}(x_{\text{tun}}, t_1^{\eta_1})]^{-\epsilon} \rangle, \end{aligned} \quad (\text{B.17})$$

and is decomposed into $\langle J_\tau^Q \rangle$ and $\langle J_\tau^N \rangle$ as

$$\langle J_\tau(t) \rangle = \langle J_\tau^Q(t) \rangle + \langle J_\tau^N(t) \rangle, \quad (\text{B.18})$$

where

$$\begin{aligned} \langle J_\tau^Q(t) \rangle &= -\frac{|\Gamma_0|^2}{8\hbar} \sum_{\eta, \eta_1=\pm 1} \sum_{\epsilon=\pm} \epsilon \eta_1 \int_{-\infty}^{\infty} dt_1 e^{i\epsilon e(V_1 - V_\nu)(t-t_1)/\hbar} \\ &\quad \times \langle T_C \left\{ v_1 \partial_x \phi_{1, H_0} |_{x=x_{\text{tun}}} + \frac{v_\nu}{\nu} \partial_x \phi_{\nu, H_0} |_{x=x_{\text{tun}}}, [\Psi_{1, H_0}^\dagger(x_{\text{tun}}, t^\eta) \Psi_{\nu, H_0}(x_{\text{tun}}, t^\eta)]^\epsilon \right\} [\Psi_{1, H_0}^\dagger(x_{\text{tun}}, t_1^{\eta_1}) \Psi_{\nu, H_0}(x_{\text{tun}}, t_1^{\eta_1})]^{-\epsilon} \rangle, \\ \langle J_\tau^N(t) \rangle &= \frac{|\Gamma_0|^2 (\mu_1 + \mu_\nu)}{4\hbar^2} \sum_{\eta, \eta_1=\pm 1} \sum_{\epsilon=\pm} \epsilon \eta_1 \int_{-\infty}^{\infty} dt_1 e^{i\epsilon e(V_1 - V_\nu)(t-t_1)/\hbar} \\ &\quad \times \langle T_C [\Psi_{1, H_0}^\dagger(x_{\text{tun}}, t^\eta) \Psi_{\nu, H_0}(x_{\text{tun}}, t^\eta)]^\epsilon [\Psi_{1, H_0}^\dagger(x_{\text{tun}}, t_1^{\eta_1}) \Psi_{\nu, H_0}(x_{\text{tun}}, t_1^{\eta_1})]^{-\epsilon} \rangle. \end{aligned} \quad (\text{B.19})$$

As we will show now, $\langle J_\tau^Q \rangle$ corresponds to tunneling heat current in the case of $e(V_1 - V_\nu) = 0$ and $\langle J_\tau^N \rangle$ corresponds to tunneling energy current associated with the tunneling charge current. Through a similar calculation to that of $\langle I_\tau(t) \rangle$ (from Eq. (B.7) to Eq. (B.12)), $\langle J_\tau^N(t) \rangle$ is easily computed as

$$\begin{aligned} \langle J_\tau^N(t) \rangle &= \frac{i(\mu_1 + \mu_\nu)|\Gamma_0|^2}{2h^2b^2} \sum_{\eta, \eta_1 = \pm 1} \eta_1 \int_{-\infty}^{\infty} dt_1 \sin\left(\frac{e}{\hbar}(V_1 - V_\nu)(t - t_1)\right) e^{G_1^{\eta\eta_1}(t-t_1)} e^{G_\nu^{\eta\eta_1}(t-t_1)/\nu^2} \\ &\simeq \frac{e}{2\hbar} g_1(\mu_1 + \mu_\nu)(V_1 - V_\nu) = g_1 \frac{\mu_1^2 - \mu_\nu^2}{2h}. \end{aligned} \quad (\text{B.20})$$

Using the relation $\langle B_1 e^{B_2} \rangle = \langle B_1 B_2 \rangle e^{\langle B_2^2 \rangle / 2}$ where B_1 and B_2 are linear operators of free bosons, $\langle J_\tau^Q(t) \rangle$ is written in terms of Green's functions of the modes as

$$\begin{aligned} \langle J_\tau^Q \rangle &= -\frac{i|\Gamma_0|^2}{4\pi\hbar b^2} \sum_{\eta, \eta_1 = \pm 1} \eta_1 \int_{-\infty}^{\infty} dt_1 \cos\left(\frac{e}{\hbar}(V_1 - V_\nu)(t - t_1)\right) e^{G_\nu^{\eta\eta_1}(t-t_1)/\nu^2} e^{G_1^{\eta\eta_1}(t-t_1)} \\ &\quad \times (v_1 \partial_x G_1^{\eta\eta_1}(x - x_{\text{tun}}, t - t_1)|_{x=x_{\text{tun}}} + \frac{v_\nu}{\nu^2} \partial_x G_\nu^{\eta\eta_1}(x - x_{\text{tun}}, t - t_1)|_{x=x_{\text{tun}}}) \\ &= -\frac{\pi|\Gamma_0|^2}{2h^2b^2} \sum_{\eta, \eta_1 = \pm 1} \eta_1 \int_{-\infty}^{\infty} dt' \cos\left(\frac{e}{\hbar}(V_1 - V_\nu)t'\right) \chi_{\eta\eta_1}(t') \left(\frac{\pi b/\hbar v_\nu \beta_\nu}{\sin[\frac{\pi}{\hbar v_\nu \beta_\nu}(b + iv_\nu t' \chi_{\eta\eta_1}(t'))]} \right)^{1/\nu} \\ &\quad \times \left(\frac{\pi b/\hbar v_1}{\sin[\frac{\pi}{\hbar v_1 \beta_1}(b + iv_1 t' \chi_{\eta\eta_1}(t'))]} \right) \left(\frac{1}{\beta_1} \frac{\cos[\frac{\pi}{\hbar v_1 \beta_1}(b + iv_1 t' \chi_{\eta\eta_1}(t'))]}{\sin[\frac{\pi}{\hbar v_1 \beta_1}(b + iv_1 t' \chi_{\eta\eta_1}(t'))]} - \frac{1}{\beta_\nu \nu} \frac{\cos[\frac{\pi}{\hbar v_\nu \beta_\nu}(b + iv_\nu t' \chi_{\eta\eta_1}(t'))]}{\sin[\frac{\pi}{\hbar v_\nu \beta_\nu}(b + iv_\nu t' \chi_{\eta\eta_1}(t'))]} \right) \\ &= -\frac{\pi|\Gamma_0|^2}{2h^2b^2} \sum_{\eta = \pm 1} \int_{-\infty}^{\infty} dt' \cos\left(\frac{e}{\hbar}(V_1 - V_\nu)t'\right) \left(\frac{\pi b/\hbar v_\nu \beta_\nu}{\sin[\frac{\pi}{\hbar v_\nu \beta_\nu}(b - i\eta v_\nu t')] } \right)^{1/\nu} \left(\frac{\pi b/\hbar v_1 \beta_1}{\sin[\frac{\pi}{\hbar v_1 \beta_1}(b - i\eta v_1 t')] } \right) \\ &\quad \times \left(\frac{1}{\beta_1} \frac{\cos[\frac{\pi}{\hbar v_1 \beta_1}(b - i\eta v_1 t')]}{\sin[\frac{\pi}{\hbar v_1 \beta_1}(b - i\eta v_1 t')]} - \frac{1}{\beta_\nu \nu} \frac{\cos[\frac{\pi}{\hbar v_\nu \beta_\nu}(b - i\eta v_\nu t')]}{\sin[\frac{\pi}{\hbar v_\nu \beta_\nu}(b - i\eta v_\nu t')]} \right). \end{aligned} \quad (\text{B.21})$$

The last equality comes from the fact that only $\chi_{\eta-\eta}(t)$ contribution to the integral survives because the $\chi_{\eta\eta}$ contribution makes the integrand odd with respect to $t = 0$. When the change of variable $t' \rightarrow t' - ib\eta/v_\nu + i\eta\hbar\beta_\nu/2$ is performed, the integral becomes simplified as

$$\begin{aligned} \langle J_\tau^Q \rangle &= -\frac{\pi|\Gamma_0|^2}{2h^2b^2} \sum_{\eta = \pm 1} \int_{-\infty + ib\eta/v_\nu - i\eta\hbar\beta_\nu/2}^{\infty + ib\eta/v_\nu - i\eta\hbar\beta_\nu/2} dt' \cos\left[\frac{e(V_1 - V_\nu)(t' + i\eta\hbar\beta_\nu/2)}{\hbar}\right] \left(\frac{\pi b/\hbar v_\nu \beta_\nu}{\sin\left(\frac{\pi}{2} - \frac{i\eta\pi t'}{\hbar\beta_\nu}\right)} \right)^{1/\nu} \\ &\quad \times \left(\frac{\pi b/\hbar v_1 \beta_1}{\sin\left[\frac{\pi}{\hbar v_1 \beta_1}\left\{b\left(1 - \frac{v_1}{v_\nu}\right) - i\eta v_1 t' + \frac{\hbar\beta_\nu v_1}{2}\right\}\right]} \right) \left(\frac{1}{\beta_1} \frac{\cos\left[\frac{\pi}{\hbar v_1 \beta_1}\left\{b\left(1 - \frac{v_1}{v_\nu}\right) - i\eta v_1 t' + \frac{\hbar\beta_\nu v_1}{2}\right\}\right]}{\sin\left[\frac{\pi}{\hbar v_1 \beta_1}\left\{b\left(1 - \frac{v_1}{v_\nu}\right) - i\eta v_1 t' + \frac{\hbar\beta_\nu v_1}{2}\right\}\right]} - \frac{1}{\beta_\nu \nu} \frac{\cos\left(\frac{\pi}{2} - \frac{i\eta\pi t'}{\hbar\beta_\nu}\right)}{\sin\left(\frac{\pi}{2} - \frac{i\eta\pi t'}{\hbar\beta_\nu}\right)} \right) \\ &= -\frac{\pi|\Gamma_0|^2}{2h^2b^2} \sum_{\eta = \pm 1} \int_{-\infty}^{\infty} dt' \cos\left[\frac{e(V_1 - V_\nu)(t' + i\eta\hbar\beta_\nu/2)}{\hbar}\right] \left(\frac{\pi b/\hbar v_\nu \beta_\nu}{\cosh(\pi t'/\hbar\beta_\nu)} \right)^{1/\nu} \\ &\quad \times \left(\frac{\pi b/\hbar v_1 \beta_1}{\sin\left(\frac{\pi\beta_\nu}{2\beta_1} - \frac{i\eta\pi t'}{\hbar\beta_1}\right)} \right) \left(\frac{1}{\beta_1 \tan\left(\frac{\pi\beta_\nu}{2\beta_1} - \frac{i\eta\pi t'}{\hbar\beta_1}\right)} - \frac{i\eta}{\beta_\nu \nu} \tanh\left(\frac{\pi t'}{\hbar\beta_\nu}\right) \right). \end{aligned} \quad (\text{B.22})$$

Let us compute $\langle J_\tau^Q \rangle$ in the first order in $\Delta T = T_1 - T_\nu$ in the limit of $|T_1 - T_\nu| \ll \bar{T}$. In addition, we ignore

the term in the second order of $(V_1 - V_\nu)$ ($O((V_1 - V_\nu)^2)$). The first order in ΔT contributes to $\langle J_\tau^Q \rangle$ as

$$\begin{aligned}
\langle J_\tau^Q \rangle &\simeq \frac{\pi^2 |\Gamma_0|^2 k_B \Delta T v_\nu}{2h^2 b^2 v_1} \left(\frac{\pi b k_B \bar{T}}{\hbar v_\nu} \right)^{1+1/\nu} \int_{-\infty}^{\infty} dt' \left(\frac{(1/\nu - 1) [\cosh(\pi k_B \bar{T} t' / \hbar)]^2 + (2 - 1/\nu)}{[\cosh(\pi k_B \bar{T} t' / \hbar)]^{1/\nu+3}} \right) \\
&= \frac{\pi^2 (k_B \bar{T}) (k_B \Delta T)}{h} \frac{1/\nu}{1/\nu + 2} \frac{(2\pi)^{\frac{1}{\nu}-1} [\Gamma(\frac{1}{2} + \frac{1}{2\nu})]^2}{\Gamma(1 + \frac{1}{\nu})} \left(\frac{|\Gamma_0|^2 / b^2}{(\hbar v_1 / b) k_B \bar{T}} \right) \left(\frac{k_B \bar{T}}{(\hbar v_\nu / b)} \right)^{\frac{1}{\nu}} \\
&= g_1 \frac{\pi^2 k_B^2 (T_1^2 - T_\nu^2)}{6h} \frac{3/\nu}{1/\nu + 2},
\end{aligned} \tag{B.23}$$

and it corresponds to the heat current in the linear response regime. Note that in the non-interacting case ($\nu = 1$), we reproduce Wiedemann-Franz law $\langle J_\tau^Q \rangle = g \pi^2 k_B^2 (T_1^2 - T_\nu^2) / 6h$. The factor $(3/\nu)/(1/\nu + 2) \neq 1$ for $\nu \neq 1$ is a correction of Wiedemann-Franz law in the quantum Hall line junction system consisting of $\delta\nu_1 = +1$ and $\delta\nu_2 = -\nu$ edge modes.

We do the similar calculation of the electric tunneling current and the energy tunneling current between downstream $\nu = 1/(2m + 1)$ and upstream $-\nu$ edge modes for $m \in Z^+$ (these correspond to modes 1 and 2 of the WMG edge structure in the main text). The only difference we have is that only quasiparticle tunneling between the edge modes is considered. The electric tunneling current $\langle I_\tau \rangle$ mode 1 to mode 2 is written as

$$\langle I_\tau \rangle = g_2 \frac{\nu e^2}{h} (V_1 - V_2), \tag{B.24}$$

where

$$g_2 = \nu (2\pi)^{(2\nu-2)} \frac{(\Gamma(\nu))^2}{\Gamma(2\nu)} \left(\frac{|\Gamma_0|/b}{k_B \bar{T}} \right)^2 \left(\frac{k_B \bar{T}}{(\hbar v_1 / b)} \right)^\nu \left(\frac{k_B \bar{T}}{(\hbar v_2 / b)} \right)^\nu, \tag{B.25}$$

$v_{1(2)}$ is the velocity of the downstream (upstream) edge mode, and $V_{1(2)}$ is applied voltage to the downstream (upstream) edge mode. The energy tunneling current $\langle J_\tau \rangle$ is written as

$$\langle J_\tau \rangle = \frac{\nu e^2}{2h} (V_1^2 - V_2^2) + g_2 \frac{\pi^2 k_B^2 (T_1^2 - T_2^2)}{6h} \frac{3\nu}{2\nu + 1}. \tag{B.26}$$

Eqs. (B.24) and (B.26) are the first equation in Eq. (32) and (39) in the main text.

Appendix C. Range of validity of approximations

The approximations made in the calculation of the tunneling currents set restrictions on the range of validity of the temperature and voltage profiles. In particular, the approximations are somewhat uncontrolled (since they must be valid at every point x), so we can only minimize their inaccuracies by putting certain restrictions on the energy scales involved. From Eqs. (B.12) and (B.29), in order for g_1, g_2 to be small, we require that

$$(|\Gamma_0|/b) \ll k_B \bar{T}(x) \ll (\hbar v/b) \tag{C.1}$$

In other words, we require that the average temperature $\bar{T}(x)$ at each point be much smaller than the bandwidth $\hbar v/b$ of the gapless modes on the edge, which are typical experimental conditions, and we also require that both

of these scales be much larger than the tunneling energy; this corresponds to the weak tunneling limit. We also note that we neglect the dependence of the g_1, g_2 on $\bar{T}(x)$, noting that from the microscopic calculations of Appendix B we have $g_1 \propto \bar{T}^2$, and $g_2 \propto \bar{T}^{-\frac{4}{3}}$. We can minimize the errors due to this approximation by requiring that:

$$\Delta T_i(x) \ll T_0, \quad (\text{C.2})$$

where $\Delta T_i(x) \equiv T_i(x) - T_0$ is the deviation from the ambient temperature T_0 on channel i .

Appendix D. Boundary conditions

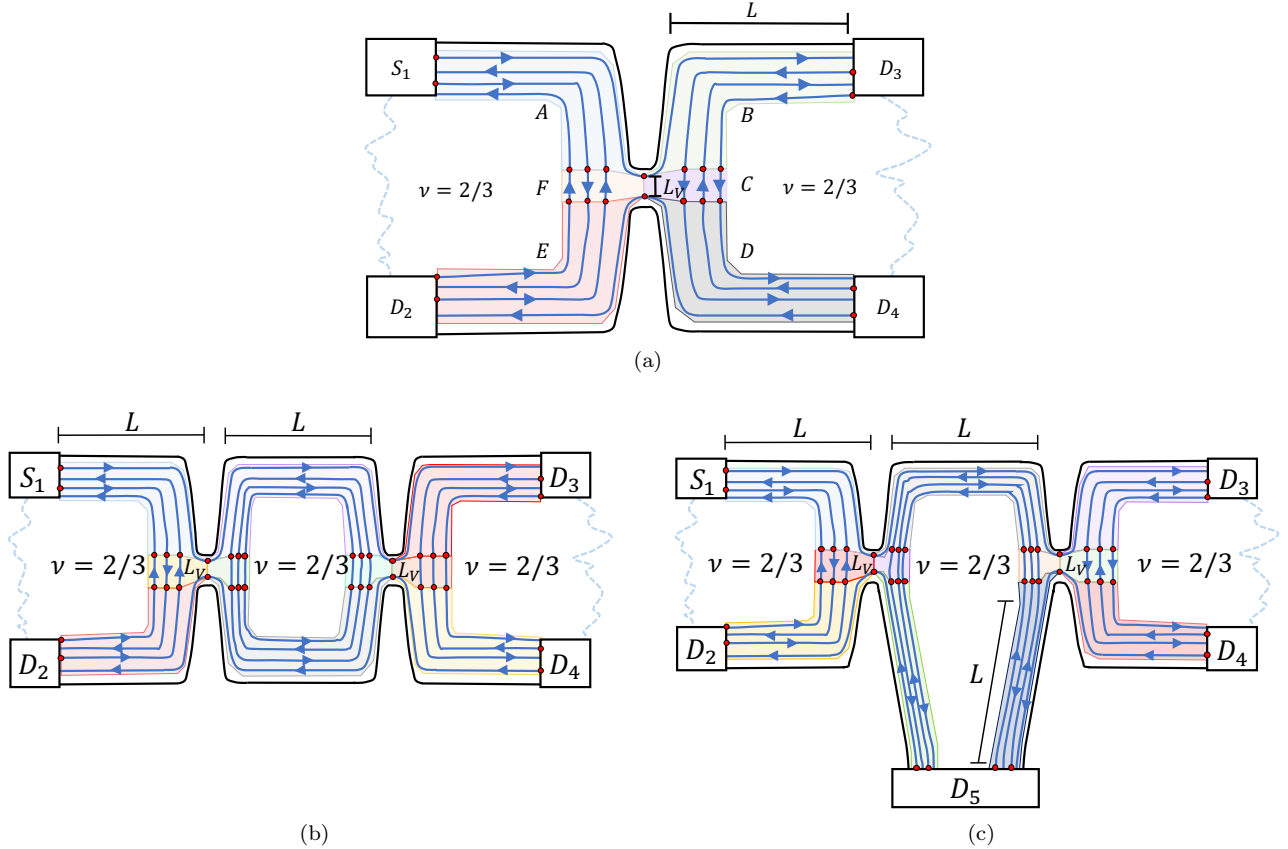


Figure D.10: (a) Single QPC geometry with points of boundary condition matching shown (red dots); there are 22 such points. The single QPC geometry consists of six different regions (A, B, C, D, E, F as shown in the figure) where the solutions are matched; these regions are indicated with translucent colorings. (b) Winding geometry with points of boundary condition matching shown (red dots); there are 36 such points. The different regions where the solutions are matched are indicated with translucent colorings. (c) No-winding geometry with points of boundary condition matching shown (red dots); there are 40 such points. The different regions where the solutions are matched are indicated with translucent colorings.

The boundary conditions are matched from the given solutions Eqs. (34), (35) in the electrical case, and Eqs. (41), (42) in the heat transport case. For example, for electrical transport in the single QPC geometry, we have 6 regions (from upper left going clockwise, we have regions A, B, C, D, E, F) to match the boundary conditions from the solutions Eqs. (34), (35). The direction of the coordinate x always follows the chirality of the $\delta\nu_3 = +1$ channel, so that in regions A, B the x coordinate goes from left to right, in region C the x coordinate goes from down to up, in regions D, E the x coordinate goes from right to left and in region F the x coordinate goes from up to down. The boundary conditions are given by the sources of the channels for each region, as shown by the red dots in Figure E.10(a); in this case, there are 22. Eventually, we get a set of coupled linear equations of the form:

$$M \cdot \vec{a} = \vec{I}_{ext}, \quad (\text{D.1})$$

with \vec{I}_{ext} as the vector of the currents induced by the external voltage V_0 , M a 22×22 matrix encoding the current matching conditions, and \vec{a} the vector of the coefficients in each region. The boundary conditions \vec{a} are plugged back into the solutions, and the conductances $G_{S_1 D_i}$ for $i = 2, 3, 4$ are given by the sum of the incoming currents to the given drains $D_{2,3,4}$, divided by the external voltage V_0 . Solving for the boundary conditions can be done analytically; however, the analytical expressions for the final conductances are intractably large and impractical to simplify, so therefore we numerically solved the system as a function of the parameters L, L_V, ℓ_1, α .

Appendix E. Charge/neutral mode description of the edge

We have the following equation for the WMG edge:

$$\frac{1}{\ell_1} \begin{pmatrix} -\alpha & -\alpha & 0 & 0 \\ \alpha & (6 + \alpha) & 3 & 3 \\ 0 & -9 & -6 & -9 \\ 0 & 3 & 3 & 6 \end{pmatrix} \begin{pmatrix} I_1(x) \\ I_2(x) \\ I_3(x) \\ I_4(x) \end{pmatrix} = \partial_x \begin{pmatrix} I_1(x) \\ I_2(x) \\ I_3(x) \\ I_4(x) \end{pmatrix}, \quad (\text{E.1})$$

which can be written in the simple form of $A\bar{I}(x) = \partial_x \bar{I}(x)$. We wish to examine the problem in the neutral mode basis for the intermediate fixed point ($\alpha \ll 1$) and the KFP fixed point ($\alpha \rightarrow \infty$).

Intermediate fixed point ($\alpha \ll 1$)

In this picture, we want to describe the problem in terms of the neutral mode basis for $\alpha = 0$. Contributions from the fact that $\alpha \neq 0$ are interpreted as effective tunneling terms.

Neutral mode basis of inner three modes

For $\alpha = 0$, we can solve the problem through diagonalization of A :

$$A = UDU^{-1}, \vec{I}(x) = U^{-1}\vec{\tilde{I}}(x)$$

$$U^{-1} = \begin{pmatrix} 0 & 1 & 1 & 2 \\ 0 & 3 & 2 & 3 \\ 0 & 1 & 1 & 1 \\ 1 & 0 & 0 & 0 \end{pmatrix}, U = \begin{pmatrix} 0 & 0 & 0 & 1 \\ -1 & 1 & -1 & 0 \\ 0 & -1 & 3 & 0 \\ 1 & 0 & -1 & 0 \end{pmatrix}, D = \begin{pmatrix} 3 & 0 & 0 & 0 \\ 0 & 3 & 0 & 0 \\ 0 & 0 & 0 & 0 \\ 0 & 0 & 0 & 0 \end{pmatrix} \quad (\text{E.2})$$

The rows of U^{-1} can directly be read off as transformations of the ϕ_i into the charge/neutral mode basis: the first and second rows are neutral modes with $\delta\tilde{\nu}_{1,2} = 0$, and the third and fourth rows are downstream charge modes with $\delta\tilde{\nu}_{3,4} = +1/3$.

We can apply the same transformation to the matrix $A(\alpha \neq 0)$, i.e. transform the problem to the charge/neutral mode basis of the incoherent fixed point; the picture that emerges is that there are effective tunneling terms between all of the modes on top of the incoherent fixed point at $\alpha = 0$:

$$U^{-1}A(\alpha)U\vec{I}(x) \equiv \tilde{A}\vec{I}(x) = \partial_x\vec{I}(x),$$

$$\frac{1}{\ell_1} \begin{pmatrix} (3-\alpha) & \alpha & -\alpha & \alpha \\ -3\alpha & 3(1+\alpha) & -3\alpha & 3\alpha \\ -\alpha & \alpha & -\alpha & \alpha \\ \alpha & -\alpha & \alpha & -\alpha \end{pmatrix} \begin{pmatrix} \tilde{I}_1(x) \\ \tilde{I}_2(x) \\ \tilde{I}_3(x) \\ \tilde{I}_4(x) \end{pmatrix} = \partial_x \begin{pmatrix} \tilde{I}_1(x) \\ \tilde{I}_2(x) \\ \tilde{I}_3(x) \\ \tilde{I}_4(x) \end{pmatrix} \quad (\text{E.3})$$

We note that the sum $\tilde{I}_3 + \tilde{I}_4$ is conserved. Solving the equation $\tilde{A}\vec{I}(x) = \partial_x\vec{I}(x)$, we get the following solution:

$$\vec{I}(x) = a_1 \begin{pmatrix} 1 \\ 1 \\ 0 \\ 0 \end{pmatrix} e^{\frac{3x}{\ell_1}} + a_2 \begin{pmatrix} 0 \\ 0 \\ -1 \\ -1 \end{pmatrix} + a_3 \begin{pmatrix} \frac{1}{6} \left(3 - \sqrt{3(3+8\alpha)} \right) \\ \frac{1}{2} \left(3 - \sqrt{3(3+8\alpha)} \right) \\ -\frac{1}{6} \left(3 + \sqrt{3(3+8\alpha)} \right) \\ \frac{1}{6} \left(3 + \sqrt{3(3+8\alpha)} \right) \end{pmatrix} e^{\frac{(3-\sqrt{3(3+8\alpha)})x}{2\ell_1}}$$

$$+ a_4 \begin{pmatrix} -\frac{1}{6} \left(3 + \sqrt{3(3+8\alpha)} \right) \\ \frac{1}{2} \left(3 + \sqrt{3(3+8\alpha)} \right) \\ -\frac{1}{6} \left(3 - \sqrt{3(3+8\alpha)} \right) \\ \frac{1}{6} \left(3 - \sqrt{3(3+8\alpha)} \right) \end{pmatrix} e^{\frac{(3+\sqrt{3(3+8\alpha)})x}{2\ell_1}} \quad (\text{E.4})$$

From Eqs. (34) and (D.4), we have that $\tilde{I}_3 + \tilde{I}_4 = I_1 + I_2 + I_3 + I_4$, as required. Thus \tilde{I}_3, \tilde{I}_4 carry all of the physical current, and are the charge modes.

The form further simplifies in the $\alpha \ll 1$ limit:

$$\vec{I}(x) \approx a_1 \begin{pmatrix} 1 \\ 1 \\ 0 \\ 0 \end{pmatrix} e^{\frac{3x}{\ell_1}} + a_2 \begin{pmatrix} 0 \\ 0 \\ -1 \\ -1 \end{pmatrix} + a_3 \begin{pmatrix} -\frac{2\alpha}{3} \\ -2\alpha \\ -1 \\ 1 \end{pmatrix} e^{-\frac{2\alpha x}{\ell_1}} + a_4 \begin{pmatrix} -1 \\ 3 \\ \frac{2\alpha}{3} \\ -\frac{2\alpha}{3} \end{pmatrix} e^{\frac{3x}{\ell_1}} \quad (\text{E.5})$$

To further understand the implications of this form for the transport results, we look at the boundary conditions in the limit that $\ell_1/L \ll 1, \alpha \ll 1$. In general, the boundary conditions can be written in the following manner:

$$\begin{aligned}
& \begin{pmatrix} 0 & -1 & \frac{1}{6} \left(3 + \sqrt{3(3+8\alpha)} \right) & \frac{1}{6} \left(3 - \sqrt{3(3+8\alpha)} \right) \\ 0 & 1 & \frac{1}{6} \left(9 - \sqrt{3(3+8\alpha)} \right) e^{\frac{(3-\sqrt{3(3+8\alpha)})L}{2\ell_1}} & \frac{1}{6} \left(9 + \sqrt{3(3+8\alpha)} \right) e^{\frac{(3+\sqrt{3(3+8\alpha)})L}{2\ell_1}} \\ -1 & -3 & -3 & -3 \\ e^{\frac{3L}{\ell_1}} & 1 & e^{\frac{(3-\sqrt{3(3+8\alpha)})L}{2\ell_1}} & e^{\frac{(3+\sqrt{3(3+8\alpha)})L}{2\ell_1}} \end{pmatrix} \begin{pmatrix} a \\ b \\ c \\ d \end{pmatrix} = \begin{pmatrix} I_1(0) \\ I_2(L) \\ I_3(0) \\ I_4(L) \end{pmatrix} \\
& \xrightarrow{\alpha \ll 1} \begin{pmatrix} 0 & -1 & 1 & -\frac{2\alpha}{\ell_1} \\ 0 & 1 & e^{-\frac{2\alpha L}{\ell_1}} & 2e^{\frac{3L}{\ell_1}} \\ -1 & -3 & -3 & -3 \\ e^{\frac{3L}{\ell_1}} & 1 & e^{-\frac{2\alpha L}{\ell_1}} & e^{\frac{3L}{\ell_1}} \end{pmatrix} \begin{pmatrix} a \\ b \\ c \\ d \end{pmatrix} = \begin{pmatrix} I_1(0) \\ I_2(L) \\ I_3(0) \\ I_4(L) \end{pmatrix}, \tag{E.6}
\end{aligned}$$

where $I_1(0), I_2(L), I_3(0), I_4(L)$ are the currents at the boundaries in the original basis; the currents in each channel are bounded by $\delta\nu_i (e^2/h) V_0$. We see from the form of the solutions that in order to suppress exponential blow up, the boundary conditions for $a, d \sim e^{-\frac{3L}{\ell_1}}$ (up to signs), and we expect then also that $b, c \sim 1$ (up to signs), without the exponential suppression. Plugging these in to the charge/neutral mode basis, the modes \tilde{I}_3, \tilde{I}_4 are charge modes with a decay term $\sim e^{-\frac{2\alpha x}{\ell_1}}$, with the long decay characterizing the tunneling between them mediated by the g_2 process; the $\sim e^{\frac{3x}{\ell_1}}$ part characteristic of the neutral mode is largely suppressed (and is additionally suppressed by α). The neutral modes are characterized by their $\sim e^{\frac{3x}{\ell_1}}$ decay, with an additional slower $\sim e^{-\frac{2\alpha x}{\ell_1}}$ decay. Thus, in the ‘‘middle’’ of a segment of the edge (within $> \ell_1$ of the edge of a boundary), we can characterize transport purely by the charge modes tunneling between each other with the long scale of $\sim e^{-\frac{2\alpha x}{\ell_1}}$, i.e. scattering length of ℓ_2 , and in the $\alpha \ll 1$ limit we can ignore the $\sim e^{\frac{3x}{\ell_1}}$ decay term in the charge modes altogether. In the case that $\ell_2 > L$, the mixing between the two downstream charge modes causes the conductance $G_{S_1 D_3}$ to deviate from $(1/3)e^2/h$; as $\ell_2 \lesssim L$, the two modes can fully equilibrate with each other, and current mixes equally between them; this is the regime where $G_{S_1 D_3} \rightarrow (2/9)e^2/h$ for the winding case, and $G_{S_1 D_3} \rightarrow (1/6)e^2/h$ for the no-winding case.

KFP fixed point ($\alpha \rightarrow \infty$)

Diagonalization of the problem leads to the following solution:

$$\begin{aligned}
\vec{I}(x) &= a_1 \begin{pmatrix} 1 \\ 0 \\ 0 \\ 0 \end{pmatrix} e^{\frac{3x}{\ell_1}} + a_2 \begin{pmatrix} 0 \\ 1 \\ 0 \\ 0 \end{pmatrix} + a_3 \begin{pmatrix} 0 \\ 0 \\ 1 \\ 0 \end{pmatrix} e^{\frac{(3-\sqrt{3(3+8\alpha)})x}{2\ell_1}} + a_4 \begin{pmatrix} 0 \\ 0 \\ 0 \\ 1 \end{pmatrix} e^{\frac{(3+\sqrt{3(3+8\alpha)})x}{2\ell_1}} \\
&\underset{\alpha \gg 1}{\approx} a_1 \begin{pmatrix} 1 \\ 0 \\ 0 \\ 0 \end{pmatrix} e^{\frac{3x}{\ell_1}} + a_2 \begin{pmatrix} 0 \\ 1 \\ 0 \\ 0 \end{pmatrix} + a_3 \begin{pmatrix} 0 \\ 0 \\ 1 \\ 0 \end{pmatrix} e^{-\frac{\sqrt{6\alpha}x}{2\ell_1}} + a_4 \begin{pmatrix} 0 \\ 0 \\ 0 \\ 1 \end{pmatrix} e^{\frac{\sqrt{6\alpha}x}{2\ell_1}} \tag{E.7}
\end{aligned}$$

From this equation, we can see that in the $\alpha \rightarrow \infty$ limit, the two lower modes become localized near the boundaries, and the electrical transport will be determined by the single $\delta\nu = +2/3$ charge mode, realizing an incoherent analogue of the KFP fixed point. The problem in the diagonal basis is of the following form:

$$A = UDU^{-1}, D = \left(\frac{1}{\ell_1}\right) \text{diag} \left[3, 0, \left(3 - \sqrt{3(3+8\alpha)}\right)/2, \left(3 + \sqrt{3(3+8\alpha)}\right)/2 \right], \quad (\text{E.8})$$

with the matrix U^{-1} of the following form:

$$U^{-1} = \begin{pmatrix} 0 & 0 & \frac{1}{2} & \frac{3}{2} \\ -\frac{1}{2} & -\frac{1}{2} & -\frac{1}{2} & -\frac{1}{2} \\ \frac{1}{4} \left(1 + \frac{3}{\sqrt{3(3+8\alpha)}}\right) & \frac{1}{4} \left(1 - \frac{9}{\sqrt{3(3+8\alpha)}}\right) & -\frac{3}{2\sqrt{3(3+8\alpha)}} & -\frac{3}{2\sqrt{3(3+8\alpha)}} \\ \frac{1}{4} \left(1 - \frac{3}{\sqrt{3(3+8\alpha)}}\right) & \frac{1}{4} \left(1 + \frac{9}{\sqrt{3(3+8\alpha)}}\right) & \frac{3}{2\sqrt{3(3+8\alpha)}} & \frac{3}{2\sqrt{3(3+8\alpha)}} \end{pmatrix}, \quad (\text{E.9})$$

At the $\alpha \rightarrow \infty$ fixed point, the essential physics happens around the constrictions, where there are counter-propagating $\delta\nu = +2/3$ and $\delta\nu = -1/3$ modes which tunnel between each other, with an additional neutral mode. To see the physics near the constriction, we wish to transform the 3×3 problem into a suitable basis. We first require that \tilde{I}_2 is a $1/3$ mode, \tilde{I}_3 is a $2/3$ mode and \tilde{I}_4 is a neutral mode. The discontinuity in the filling factor is given by $\delta\nu_i = \sum_j t_i K_{ij}^{-1} t_j$, so that under the change of basis we require that:

$$\begin{aligned} \delta\tilde{\nu}_2 &= \sum_j \tilde{t}_2 \tilde{K}_{ij}^{-1} \tilde{t}_j = -\frac{1}{3} \\ \delta\tilde{\nu}_3 &= \sum_j \tilde{t}_3 \tilde{K}_{ij}^{-1} \tilde{t}_j = +\frac{2}{3} \\ \delta\tilde{\nu}_4 &= \sum_j \tilde{t}_4 \tilde{K}_{ij}^{-1} \tilde{t}_j = 0 \end{aligned} \quad (\text{E.10})$$

Additionally, we restrict the charges of the neutral mode and the $-1/3$ mode excitations:

$$\begin{aligned} \tilde{Q}_3 &= (-e) \sum_{ij} (U_{3 \times 3})_{2i}^{-1} K_{ij}^{-1} t_j = \frac{e}{3} \\ \tilde{Q}_4 &= (-e) \sum_{ij} (U_{3 \times 3})_{3i}^{-1} K_{ij}^{-1} t_j = 0 \end{aligned} \quad (\text{E.11})$$

Finally, we require local current conservation between the two charge modes: this forces the matrix $A_{3 \times 3}$ in its most general form to be:

$$\tilde{A}_{3 \times 3} = U^{-1} A_{3 \times 3} U = \frac{1}{\ell_1} \begin{pmatrix} a & b & c \\ -a & -b & -c \\ d & e & f \end{pmatrix} \quad (\text{E.12})$$

for some undetermined constants a, b, c, d, e, f . Putting these constraints together, we find that $\tilde{A}_{3 \times 3} = \frac{1}{\ell_1} \begin{pmatrix} 6 & 3 & 0 \\ -6 & -3 & 0 \\ 0 & 0 & 3 \end{pmatrix}$. Additionally, we require that the transformation obeys global current conservation:

$$\tilde{I}_2 + \tilde{I}_3 = I_2 + I_3 + I_4 \quad (\text{E.13})$$

The solution of the untransformed equation $A_{3 \times 3} \vec{I}(x) = \partial_x \vec{I}(x)$ is

$$\vec{I}(x) = b_1 \begin{pmatrix} -1 \\ 0 \\ 1 \end{pmatrix} e^{\frac{3x}{\ell_1}} + b_2 \begin{pmatrix} -1 \\ 1 \\ 0 \end{pmatrix} e^{\frac{3x}{\ell_1}} + b_3 \begin{pmatrix} 1 \\ -3 \\ 1 \end{pmatrix}. \quad (\text{E.14})$$

Following the aforementioned constraints, the transformed solution becomes:

$$\vec{\tilde{I}}(x) = \frac{b_1}{X} \begin{pmatrix} (u_3 + u_9) \\ -(u_3 + u_9) \\ -(2 + u_2 + u_8) \end{pmatrix} e^{\frac{3x}{\ell_1}} + \frac{b_2}{X} \begin{pmatrix} u_9 \\ -u_9 \\ -(1 + u_8) \end{pmatrix} e^{\frac{3x}{\ell_1}} + b_3 \begin{pmatrix} 1 \\ -2 \\ 0 \end{pmatrix}, \quad (\text{E.15})$$

with

$$U_{3 \times 3} = \begin{pmatrix} 1 + 2u_2 & u_2 & u_3 \\ -(1 + 2u_2 + 2u_8) & (1 - u_2 - u_8) & -(u_3 + u_9) \\ 1 + 2u_8 & u_8 & u_9 \end{pmatrix}, \quad (\text{E.16})$$

and $X \equiv u_3(1 + u_8) - u_9(1 + u_2)$. Solving for $\vec{\tilde{I}}(x)$ and $U_{3 \times 3}$ fully requires matching boundary conditions in the new basis, which is prohibitively difficult (as it will involve expressing the solution in terms of the original coefficients, which are complicated). The main observations about Eq. (D.15) are that: (1) the neutral mode consists of a purely decaying part with decay length $\ell_1/3$, which is a reflection of the decoupling of the neutral mode from the charge modes in $\tilde{A}_{3 \times 3}$, (2) the tunneling between the charge modes $\delta\tilde{\nu}_2, \delta\tilde{\nu}_3$ induces equilibration while the sum $\tilde{I}_2 + \tilde{I}_3 = I_2 + I_3 + I_4$ as required, and (3) in the absence of tunneling between charge modes, the charge modes obey the condition that $\tilde{I}_2 = -2\tilde{I}_3$, which is a reflection of the restriction on the filling factors $\delta\tilde{\nu}_2 = -1/3, \delta\tilde{\nu}_3 = +2/3$.

References

References

- [1] B. I. Halperin, *Quantized hall conductance, current-carrying edge states, and the existence of extended states in a two-dimensional disordered potential*, Phys. Rev. B **25**, 2185 (1982).
- [2] X. G. Wen, *Chiral luttinger liquid and the edge excitations in the fractional quantum hall states*, Mod. Phys. Lett. **5**, 39 (1991).
- [3] A. H. MacDonald, *Edge states in the fractional-quantum-hall-effect regime*, Phys. Rev. Lett. **64**, 220 (1990).
- [4] Y. Meir, *Composite edge states in the $\nu = 2/3$ fractional quantum hall regime*, Phys. Rev. Lett. **72**, 2624 (1994).
- [5] J. Wang, Y. Meir and Y. Gefen, *Edge reconstruction in the $\nu = 2/3$ fractional quantum hall state*, Phys. Rev. Lett. **111**, 246803 (2013).
- [6] X. G. Wen, *Chiral luttinger liquid and the edge excitations in the fractional quantum hall states*, Phys. Rev. B **41**, 12838 (1990); X.G. Wen, *Gapless boundary excitations in the quantum hall states and in the chiral spin state*, Phys. Rev. B **43**, 11025 (1991).

- [7] M. Reznikov, R. de Picciotto, T. G. Griffiths, M. Heiblum, and V. Umansky, *Observation of quasiparticles with one-fifth of an electron's charge*, Nature **399**, 238 (1995); M. Dolev, M. Heiblum, V. Umansky, A. Stern, and D. Mahalu, *Observation of a quarter of an electron charge at the $\nu = 5/2$ quantum hall state*, Nature **452**, 829 (2008).
- [8] C. L. Kane and M. P. A. Fisher, *Transmission through barriers and resonant tunneling in an interacting one-dimensional electron gas*, Phys. Rev. B **46**, 15233 (1992).
- [9] F. P. Milliken, C. P. Umbach, and R. A. Webb, *Indications of a luttinger liquid in the fractional quantum hall regime*, Solid State Communications **97**, 309 (1996).
- [10] F. D. M. Haldane, *Fractional quantization of the hall effect: A hierarchy of incompressible quantum fluid states*, Phys. Rev. Lett. **51**, 605 (1983); B. I. Halperin, *Statistics of quasiparticles and the hierarchy of fractional quantized hall states*, Phys. Rev. Lett. **52**, 1583 (1984).
- [11] S. M. Girvin, *Particle-hole symmetry in the anomalous quantum hall effect*, Phys. Rev. B **29**, 6012 (1984).
- [12] R. C. Ashoori, H. L. Stormer, L. N. Pfeiffer, K. W. Baldwin, and K. West, *Edge magnetoplasmons in the time domain*, Phys. Rev. B **45**, 3894, (1992).
- [13] C. L. Kane, M. P. A. Fisher and J. Polchinski, *Randomness at the edge: Theory of quantum hall transport at filling $\nu = 2/3$* , Phys. Rev. Lett. **72**, 4129, (1994).
- [14] A. Bid, N. Ofek, H. Inoue, M. Heiblum, C. L. Kane, V. Umansky, and D. Mahalu, *Observation of neutral modes in the fractional quantum hall regimes*, Nature **466**, 585 (2010); H. Inoue, A. Grivnin, Y. Ronen, M. Heiblum, V. Umansky, and D. Mahalu, *Proliferation of neutral modes in fractional quantum hall states*, Nature Communications **5**, 1 (2014).
- [15] J. Park, Y. Gefen, and H.-S. Sim, *Topological dephasing in the $\nu = 2/3$ fractional quantum Hall regime*, Phys. Rev. B **92**, 245437 (2015).
- [16] M. Goldstein and Y. Gefen, *Suppression of Interference in Quantum Hall Mach-Zehnder Geometry by Upstream Neutral Modes*, Phys. Rev. Lett. **117**, 276804 (2016).
- [17] M. Carrega, D. Ferraro, A. Braggio, N. Magnoli, and M. Sassetti, *Anomalous charge tunneling in the fractional quantum Hall edge states at filling factor $\nu = 5/2$* , Phys. Rev. Lett. **107**, 146404 (2012).
- [18] A. Braggio, D. Ferraro, M. Carrega, N. Magnoli, and M. Sassetti, *Environmental induced renormalization effects in quantum Hall edge states due to $1/f$ noise and dissipation*, New Journal of Physics, **14**, 093032 (2012).
- [19] A. M. Chang and J. E. Cunningham, *Transport evidence for phase separation into spatial regions of different fractional quantum hall fluids near the boundary of a two-dimensional electron gas*, Phys. Rev. Lett. **69**, 2114 (1992).
- [20] Aveek Bid, N. Ofek, M. Heiblum, V. Umansky, and D. Mahalu, *Shot noise and charge at the $\nu = 2/3$ composite fractional quantum hall state*, Phys. Rev. Lett. **103**, 236802 (2009).
- [21] R. Sabo, I. Gurman, A. Rosenblatt, F. Lafont, D. Banitt, J. Park, M. Heiblum, Y. Gefen, V. Umansky, and D. Mahalu, *Edge reconstruction in fractional quantum Hall states*, Nature Phys. **13**, 491 (2017).

- [22] J. E. Moore and X. G. Wen, *Classification of disordered phases of quantum hall edge states*, Phys. Rev. B **57**, 10138 (1998); J. E. Moore and X. G. Wen, *Critical points in edge tunneling between generic fractional quantum hall states*, Phys. Rev. B **66**, 115305, (2002).
- [23] B. Rosenow and B. I. Halperin, *Signatures of neutral quantum hall modes in transport through low- density constrictions*, Phys. Rev. B **81**, 165313 (2010).
- [24] I.V. Protopopov, Y. Gefen and A.D. Mirlin, *Transport in a disordered $\nu = 2/3$ fractional quantum Hall junction*, Annals of Physics **385**, 287 (2017).
- [25] C. L. Kane and M. P. A. Fisher, *Contacts and edge-state equilibration in the fractional quantum hall effect*, Phys. Rev. B **52**, 17393, (1995).
- [26] C. L. Kane and M. P. A. Fisher, *Quantized thermal transport in the fractional quantum hall effect*, Phys. Rev. B **55**, 15832, (1997).
- [27] D. Sen and A. Agarwal, *Line junction in a quantum hall system with two filling fractions*, Phys. Rev. B **78**, 085430, (2008).
- [28] M. Levin, B. Rosenow and B.I. Halperin, *Particle-hole Symmetry and the Pfaffian State*, Phys. Rev. Lett. **99**, 236806, (2007).
- [29] S. Lee, S. Ryu, C. Nayak and M. P. A. Fisher, *Particle-hole Symmetry and the $\nu = 5/2$ Quantum Hall State*, Phys. Rev. Lett. **99**, 236807 (2007).
- [30] V. Venkatachalam, S. Hart, L. Pfeiffer, K. West, A. Yacoby, *Local thermometry of neutral modes on the quantum hall edge*, Nature Physics **8**, 676, (2012).
- [31] C. Altimiras, H. le Sueur, U. Gennser, A. Anthore, A. Cavanna, D. Mailly, and F. Pierre, *Chargeless Heat Transport in the Fractional Quantum Hall Regime*, Phys. Rev. Lett. **109**, 026803 (2012).
- [32] M. Banerjee, M. Heiblum, A. Rosenblatt, Y. Oreg, D. E. Feldman, A. Stern and V. Umansky, *Observed quantization of anyonic heat flow*, Nature **545**, 75 (2017).
- [33] A. Rosenblatt, F. Lafont, I. Levkivskiy, R. Sabo, I. Gurman, D. Banitt, M. Heiblum and V. Umansky, *Transmission of heat modes across a potential barrier*, Nature Communications **8**, 2251 (2017).
- [34] S. Takei, B. Rosenow, *Neutral mode heat transport and fractional quantum Hall shot noise*, Phys. Rev. B **84**, 235316 (2011).
- [35] S. Takei, B. Rosenow, A. Stern, *Noise due to neutral modes in the $\nu = 2/3$ fractional quantum Hall state*, Phys. Rev. B **91**, 241104 (2015).
- [36] O. Shtanko, K. Snizkho, V. Cheianov, *Nonequilibrium noise in transport across a tunneling contact between $\nu = 2/3$ fractional quantum Hall edges*, Phys. Rev. B **89**, 125104 (2014).
- [37] M. Banerjee, M. Heiblum, V. Umansky, D. E. Feldman, Y. Oreg and A. Stern, *Observation of half-integer thermal Hall conductance*, arXiv:1710.00492 (2018).
- [38] This matches with the results of Refs. [23, 27].

- [39] K. E. Nagaev, *Influence of electron-electron scattering on shot noise in diffusive contacts*, Phys. Rev. B **52**, 4740, (1995).
- [40] M. Büttiker, *Absence of backscattering in the quantum hall effect in multiprobe conductors*, Phys. Rev. B **38**, 9375, (1988).
- [41] Y. Ronen, Y. Cohen, D. Banitt, M. Heiblum and V. Umansky, *Robust integer and fractional helical modes in the quantum Hall effect*, Nature Physics, (2018).
- [42] C. L. Kane and M. P. A. Fisher, *Thermal transport in a luttinger liquid*, Phys. Rev. Lett. **76**, 3192, (1996).
- [35] We note that while our numerical parameters clearly violate the condition that $g_1, g_2 \ll 1$, this is not a problem, since in principle all of the lengths in the problem can be rescaled by some factor c , such that $g_1 \rightarrow g_1/c, g_2 \rightarrow g_2/c$, and $g_1/c, g_2/c \ll 1$, and this rescaling will not change any of the calculable results.
- [43] C. Altimiras, H. le Sueur, U. Gennser, A. Cavanna, D. Mailly, and F. Pierre, *Non-equilibrium edge-channel spectroscopy in the integer quantum Hall regime*, Nature **6**, 34, (2010).
- [44] H. le Sueur, C. Altimiras, U. Gennser, A. Cavanna, D. Mailly, and F. Pierre, *Energy Relaxation in the Integer Quantum Hall Regime*, Phys. Rev. Lett. **105**, 056803, (2010).
- [45] I. Gurman, R. Sabo, M. Heiblum, V. Umansky, and D. Mahalu, *Extracting net current from an upstream neutral mode in the fractional quantum Hall regime*, Nature Communications **3**, 1289 (2012).
- [46] T. Martin, *Noise in Mesoscopic Physics, Proceedings of the Les Houches Summer School, Session LXXXI, edited by H. Bouchiat et al. (Elsevier, New York, 2005).*